UNIVERSIDADE
BEIRA INTERIOR

Efficient Management of Flexible Functional Splits in 5G Second Phase Networks

Ivan Micael Vicente Pires

Dissertação para obtenção do Grau de Mestre em
Engenharia Eletrotécnica e de Computadores
(2º ciclo de estudos)

Orientador: Prof. Doutor Fernando José da Silva Velez

outubro de 2022

Declaração de Integridade

Eu, (identificação), que abaixo assino, estudante com o número de inscrição (indicar) de/o (identificação do curso) da Faculdade (indicar), declaro ter desenvolvido o presente trabalho e elaborado o presente texto em total consonância com o **Código de Integridades da Universidade da Beira Interior**.

Mais concretamente afirmo não ter incorrido em qualquer das variedades de Fraude Académica, e que aqui declaro conhecer, que em particular atendi à exigida referenciação de frases, extratos, imagens e outras formas de trabalho intelectual, e assumindo assim na íntegra as responsabilidades da autoria.

Universidade da Beira Interior, Covilhã 05 / 10 /2022

Ivan Micael Vicente Pires

(assinatura conforme Cartão de Cidadão ou preferencialmente assinatura digital no documento original se naquele mesmo formato)

Acknowledgements

I would like to acknowledge my supervisor Prof. Doctor Fernando José da Silva Velez for all the knowledge and guidance shared during this journey. I would also like to thank everyone who worked with me in the lab, for their support and help in whatever was needed, especially the engineer Rui Paulo for everything he taught me. I would also like to give special thanks to my family for the strength they gave me throughout my academic life, who always helped and encouraged me to do my best. To my group of friends from Covilhã, for everything they did for me, for our friendship and for all this academic journey, they will be forever remembered. To my group of friends from Sardoal, who were always there for me and supported me. A special thanks to my girlfriend, Maria Paula, for helping me so much and for supporting me unconditionally and keeping me always with my head up and focused on my goals.

Abstract

The fifth mobile network generation (5G), which offers better data speeds, reduced latency, and a huge number of network connections, promises to improve the performance of the cellular network in practically every way available. A portion of the network operations are deployed in a centralized unit in the 5G radio access network (RAN) partially centralized design. By centralizing these functions, operational expenses are decreased and coordinating strategies are made possible. To link centralized units (CU) and distributed units (DU), and the DU to remote radio units (RRU), both the midhaul and fronthaul networks must have higher capacity. The necessary fronthaul capacity is also influenced by the fluctuating instantaneous user traffic. Consequently, the 5G RAN must be able to dynamically change its centralization level to the user traffic to maximize its performance. To try to relieve this fronthaul capacity it has been considered a more flexible distribution between the base band unit (BBU) (or CU and DU if enhanced common public radio interface (eCPRI) is considered) and the RRU. It may be challenging to provide high-speed data services in crowded areas, particularly when there is imperfect coverage or significant interference. Because of this, the macrocell deployment is insufficient. This problem for outdoor users could be resolved by the introduction of low-power nodes with a limited coverage area. In this context, this MSc dissertation explores, in an urban micro cell scenario model A (UMi_A) for three frequency bands (2.6 GHz, 3.5 GHz, and 5.62 GHz), the highest data rate achievable when a numerology zero is used. For this, it was necessary the implementation of the UMi_A in the 5G-air-simulator. Allowing the determination of the saturation level using the results for the packet loss ratio (PLR=2%). By assuming Open RAN (O-RAN) and functional splitting, the performance of two schedulers in terms of quality-of-service (QoS) were also studied. The QoS-aware modified largest weighted delay first (M-LWDF) scheduler and the QoS-unaware proportional fair (PF) scheduler. PLR was evaluated for both schedulers, whilst analyzing the impact of break point distance while changing the frequency band. The costs, revenues, profit in percentage terms, and other metrics were also estimated for the PF and M-LWDF schedulers when used video (VID) and video plus best effort (VID+BE), with or without consideration of the functional splits 7.2 and 6, for the three frequency bands. One concluded that the profit in percentage terms with functional split option 7.2 applied is always slightly higher than with functional split option 6. It reaches a maximum profit of 366.92% in the case of the M-LWDF scheduler, and 305.51% in the case of the PF scheduler, at a cell radius of 0.4 km for the 2.6 GHz frequency band, considering a price of the traffic of 0.0002 €/min.

Keywords

5G, Small Cells, 5G-Air-Simulator, Functional Splits, Cost/Revenue Trade-off, Open RAN, Fairness, Goodput, Performance Evaluation, Packet Loss Ratio, Delay.

Resumo

A quinta geração de redes móveis (5G), oferece ritmos de transmissão melhorados, atraso extremo-a-extremo reduzido, e um vasto número de ligações de rede. A 5G promete melhorar o desempenho das redes celulares em praticamente todos os aspectos relevantes. Uma parte da operação da rede é colocada numa unidade centralizada na rede de acesso de rádio (RAN) 5G com dimensionamento parcialmente centralizado. Ao centralizar estas funções, os custos operacionais decrescem, viabilizando-se as estratégias de coordenação. Para ligar as unidades centralizadas e unidades distribuídas, e por sua vez, unidades distribuidas e unidades de rádio remotas, ambos os $midhaul$ e $fronthaul$ devem ter uma capacidade mais elevada. A capacidade da $fronthaul$ necessária é também influenciada pela flutuação do tráfego instantâneo dos utilizadores. Consequentemente, a RAN 5G deve ser capaz de alterar dinamicamente o seu nível de centralização para o tráfego de utilizadores, com objetivo de maximizar o seu desempenho. Para tentar aliviar o aumento da capacidade suportada pelo $fronthaul$, tem sido considerada uma distribuição mais flexível entre a unidade de banda base, BBU (ou unidade central e unidade distribuída se a interface de rádio pública comum melhorada, eCPRI, for considerada), e a unidade de rádio remota, RRU. Em áreas densamente povoadas, pode ser um desafio fornecer serviços de dados de elevada velocidade, particularmente quando existe uma cobertura deficiente ou interferência significativa. Por este motivo, o desenvolvimento de macrocélulas pode ser insuficiente, mas este problema para utilizadores em ambiente de exterior pode ser mitigado com a introdução de nós de potência reduzida com uma área de cobertura limitada. Neste contexto, esta dissertação de mestrado explora, num cenário urbano de microcélulas caracterizado pelo modelo A (UMi_A) para três bandas de frequência (2.6 GHz, 3.5 GHz, e 5.62 GHz), o débito binário máximo que se pode alcançar quando se utiliza numerologia zero. Para tal, foi necessária a implementação do UMi_A no $5G-air-simulator$. Determinou-se o nivel de saturação, considerando-se os resultados para a taxa de perda de pacotes (PLR=2%). Estudou-se o desempenho de dois escalonadores de pacotes em termos de qualidade de serviço (QoS), assumindo-se o $OpenRAN$ (O-RAN) e as divisões funcionais ($functionalsplitting$). Um dos escalonadores é ciente da QoS, e é de atraso máximo-superior ponderado primeiro (M-LWDF), enquanto que o outro não é ciente da QoS, e é de justiça proporcional (PF). Avaliou-se o PLR para ambos os escalonadores de pacotes, estudando-se o impacto da distância de ponto de quebra ($breakpointdistance$), variando-se a banda de frequências. Foram também estimados os custos, proveitos, o lucro (em percentagem), e outras metricas, para os escalonadores PF e M-LWDF, considerando o vídeo (VID) e vídeo mais $besteffort$ (VID+BE) como aplicações, com ou sem a consideração das divisões funcionais 7.2 e 6, para as três bandas de frequência. Concluiu-se que o lucro em termos percentuais, com a escolha da opção de divisão funcional 7.2, é sempre ligeiramente mais elevado do que com a opção de divisão funcional 6. Atinge-se um lucro máximo de 366,92% no caso do escalonador M-LWDF, e de 305,51% no caso do escalonador PF, para um raio de célula de 0,4 km, para a banda de frequência de 2,6 GHz, considerando-se um preço do tráfego de 0,0002 €/min.

Palavras-chave

5G, Pequenas Células, 5G-Air-Simulator, Divisões Funcionais, Custos/Proveitos, Open RAN, Equidade, Débito Binário, Avaliação de Desempenho, Taxa de Perda de Pacotes, Atraso

Contents

1 Introduction **1**

1.1 Motivation . . . 1
1.2 Evolution of Mobile Wireless Communication Networks . . . 2
1.3 3rd Generation Partnership Project . . . 3
1.4 Heterogeneous Networks . . . 5
1.5 Objectives and Approach . . . 6
1.6 Contributions . . . 6
1.7 Outline of the Dissertation . . . 6

2 State of the Art and General Concepts **9**

2.1 Introduction . . . 9
2.2 5G RAN System Architecture . . . 9
2.3 Common Public Radio Interface and Enhanced Common Public Radio Interface 11
2.4 Functional Splits . . . 13
2.4.1 RF-PHY Split (option 8) . . . 14
2.4.2 Intra PHY Split (option 7) . . . 15
2.4.3 MAC-PHY Split (option 6) . . . 15
2.4.4 Intra MAC Split (option 5) . . . 16
2.4.5 RLC-MAC Split (option 4) . . . 16
2.4.6 Intra RLC Split (option 3) . . . 16
2.4.7 PDCP-RLC Split (option 2) . . . 17
2.4.8 RRC-PDCP Split (option 1) . . . 17
2.5 Open RAN . . . 17
2.5.1 Split Option 7.2x . . . 17
2.5.2 O-RAN Architecture . . . 18
2.5.3 Benefits of O-RAN . . . 20
2.6 Frequency Ranges . . . 20
2.7 Propagation Model . . . 21
2.8 Path Loss Model . . . 22
2.9 Supported Throughput Formulation . . . 23

3 Simulator Characterization and Performance Evaluation **27**

3.1 5G-Air-Simulator . . . 27
3.2 Capacity and Quality of Service . . . 27
3.2.1 Scheduling . . . 28
3.3 Radio and Simulation Parameters . . . 30
3.4 Results At The Saturation Level . . . 33
3.4.1 Saturation Level For Video . . . 34
3.4.2 Saturation Level with Video plus Best Effort . . . 40
3.4.3 Lessons learned about the Saturation Level . . . 41

3.5 Results for the Maximum Cell Goodput with only BE 42
3.6 Costs/Revenue Trade-off 44
3.6.1 Lessons Learned 49

4 Conclusions and Topics for Further Research **51**
4.1 Conclusions 51
4.2 Proposals of further research 52

References **55**

List of Figures

Figure 1.1 Total global monthly network data traffic from Q1 of 2015 to Q1 of 2022, along with the year-on-year percentage change. 3
Figure 1.2 Timeline of 3GPP 5G Releases from Q1 of 2019 to Q4 of 2022. 4
Figure 1.3 Different areas of the small cells and macro cells. 5

Figure 2.1 D-RAN Architecture, that consists of the link (fronthaul) between the RRU and the BBU inside the cell site, and the connection (backhaul) between the BBU and the Core Network. 10
Figure 2.2 C-RAN Architecture, formed by the RRU inside the cell site with the link (fronthaul) to the BBU pool, which is then connected (backhaul) to the Core Network. 10
Figure 2.3 Basic architecture of a CPRI based RAN, in which there is a connection between the RE and the REC. 12
Figure 2.4 Basic eCPRI structure, which presents a link, through the fronthaul, between the eREC and the eRE. 12
Figure 2.5 Different functional splits proposed by 3GPP. 13
Figure 2.6 Fronthaul bit rates for each functional split option in UL and DL. . . . 14
Figure 2.7 O-RAN architecture by ORAN Alliance. 19
Figure 2.8 Definition of d_{2D} and d_{3D} for outdoor UTs 22

Figure 3.1 Building blocks of the 5G-air-simulator. 28
Figure 3.2 Nineteen microcells in hexagonal layout, where the own central cell and the interferer cells are represented in yellow. 30
Figure 3.3 Cell of interest and interferer cells. Users are uniformly deployed in the central cell. 31
Figure 3.4 Results for the average PLR for the M-LWDF scheduler, as a function of R, with the number of users as a parameter (for different frequency bands). VID trace bit rate of 3.1 Mb/s. 34
Figure 3.5 Results for the average PLR for the PF scheduler as a function of R, with the number of users as a parameter (for different frequency bands). VID trace bit rate of 3.1 Mb/s. 35
Figure 3.6 Results for the maximum average delay for the M-LWDF scheduler as a function of R with the number of users as a parameter (for different frequency bands). VID trace bit rate of 3.1 Mb/s. 36
Figure 3.7 Results for the maximum average delay for the PF scheduler as a function of R with the number of users as a parameter (for different frequency bands). VID trace bit rate of 3.1 Mb/s. 37
Figure 3.8 Maximum average fairness index for M-LWDF and PF schedulers, Only VID trace 3.1 Mb/s. 38

Figure 3.9 Maximum average goodput for M-LWDF and PF schedulers, Analytical, VID and VID+BE. 39
Figure 3.10 Equivalent supported throughput for the 2.6, 3.5 and 5.62 GHz frequency bands, for values of cell radius up to 1 km. 40
Figure 3.11 Average fairness index for M-LWDF and PF schedulers, VID+BE trace at 3.1 Mb/s. 41
Figure 3.12 Results for the maximum performance of the simulator. Only 10 BE flows are considered. 43
Figure 3.13 Five viewpoints of the economics of cellular networks. 44
Figure 3.14 Profit for PF and M-LWDF schedulers in VID and VID+BE. 47

List of Tables

Table 2.1 Radio and simulation parameters for UMi_A 23
Table 2.2 TBS for 5G for $N_{info} \leq 3824$ 25

Table 3.1 Radio and Simulation Parameters 32
Table 3.2 Radio and Simulation Parameters for UMi_A 47

List of Acronyms

1G	First Generation
2G	Second Generation
3D	Three-Dimensional Space
3G	Third Generation
3GPP	3rd Generation Partnership Project
4G	Fourth Generation
5G NR	Fifth Generation New Radio
5G	Fifth Generation
AI	Artificial Intelligence
ARIB	Association of Radio Industries and Businesses
ARQ	Automatic Repeat Request
ATIS	Alliance for Telecommunications Industry Solutions
BBU	Baseband Unit
BE	Best Effort
BH	Backhaul
BS	Base Station
CAPEX	Capital Expenditure
CCSA	China Communications Standards Association
CN	Core Network
CoMP	Coordinated Multi-Point transmission and reception
CPRI	Common Public Radio Interface
C-RAN	Cloud Radio Access Network
CSI	Channel State Information
CU	Central Unit
DL	Downlink
D-RAN	Distributed Radio Access Network

DSL	Digital Subscriber Line
DSS	Dynamic Spectrum Sharing
DU	Distributed Unit
eCPRI	Enhanced Common Public Radio Interface
eMBB	Enhanced Mobile Broadband
eNB	Evolved Node B
eRE	Enhanced Common Public Radio Interface Radio Equipment
eREC	Enhanced Common Public Radio Interface Radio Equipment Control
ETSI	European Telecommunications Standards Institute
FFT	Fast Fourier Transform
FH	Fronthaul
FI	Fairness Index
FR1	Frequency Range 1
FR2	Frequency Range 2
gNB	Next Generation Node B
HARQ	Hybrid Automatic Repeat Request
HetNets	Heterogeneous Networks
IFFT	Inverse Fast Fourier Transform
IMT	International Mobile Telecommunications
IMT-2020	International Mobile Telecommunications 2020
IoT	Internet of Things
IQ	In-phase and Quadrature
ISD	Inter Site Distance
ITU	International Telecommunication Union
ITU-R	International Telecommunication Union Radiocommunication Sector
IWF	Interworking Function
KPI	Key Performance Indicator
L2S	Link-To-System

LoS	Line-of-Sight
LTE	Long Term Evolution
MAC	Medium Access Control
MBS	Multicast and Broadcast Service
MIESM	Mutual Information Effective Signal to Interference and Noise Ratio Mapping
MIMO	Multiple Input Multiple Output
ML	Machine Learning
M-LWDF	Modified Largest Weighted Delay First
MMB	Mobile Broadband
mMIMO	Massive Multiple Input Multiple Output
mMTC	Massive Machine Type Communications
mmW	Millimeter Wave
Near-RT RIC	Near-Real-Time Radio Access Network Intelligent Controller
Non-RT RIC	Non-Real-Time Radio Access Network Intelligent Controller
NS	Network Slicing
NSA	Non-Standalone
NTN	Non-terrestrial Network
O-CU-CP	Open Radio Access Network Central Unit Control Plane
O-CU-UP	Open Radio Access Network Central Unit User Plane
O-DU	Open Radio Access Network Distributed Unit
O-eNB	Open Radio Access Network Evolved Node B
OFDM	Orthogonal Frequency Division Multiplexing
OPEX	Operational Expenditure
O-RAN	Open Radio Access Network
O-RU	Open Radio Access Network Radio Unit
PDCP	Packet Data Convergence Protocol
PDU	Protocol Data Unit
PF	Proportional Fair

PHY	Physical Layer
PLM	Path Loss Model
PLR	Packet Loss Ratio
PRB	Physical Resource Block
Q1	First Quarter
QoE	Quality of Experience
QoS	Quality of Service
RAN	Radio Access Network
rAPP	Radio Access Network Automation Applications
RAT	Radio Access Technology
RE	Radio Equipment
REC	Radio Equipment Control
RedCap	Reduced Capability
RF	Radio Frequency
RIT	Radio Interface Technologies
RLC	Radio Link Control
RRC	Radio Resource Control
RRH	Remote Radio Head
RRM	Radio Resource Management
RRU	Remote Radio Units
RU	Remote Unit
SA	Standalone
SCS	Sub Carrier Spacing
SDAP	Service Data Adaptation Protocol
SDU	Service Data Unit
SINR	Signal to Interference and Noise Ratio
SL	Sidelink
SMO	Service Management and Orchestration

SRIT	Sets of Radio Interface Technologies
SS-PLM	Single-Slope Path Loss Model
TBS	Transport Block Size
TS	Technical Specification
TSDSI	Telecommunications Standards Development Society India
TS-PLM	Two-Slope Path Loss Model
TTA	Telecommunications Technology Association
TTC	Telecommunication Technology Committee
UE	User Equipment
UL	Uplink
UMi	Urban Micro Scenario
UMi_A	Urban Micro Scenario Model A
URLLC	Ultra-Reliable Low Latency Communications
UT	User Terminal
VID	Video
VID+BE	Video plus Best Effort

Chapter 1

Introduction

1.1 Motivation

The cloud-radio access network (C-RAN) is one of the groundbreaking wireless communications technologies of the last couple of years.
C-RAN is frequently used by telecommunication operators mainly due to its positive effects on network performance, user admission, energy efficiency, and proportional fairness [1]. The C-RAN concept supports the separation of baseband units (BBUs) from remote radio heads (RRHs), which are consolidated in one location or even virtualized in the cloud. The backhaul (BH) network refers to the link between BBUs and the core network (CN), whereas the fronthaul (FH) network refers to the connection between BBUs and RRHs. The FH huge capacity requirements are a major barrier to the C-RAN deployment. In order to try to relieve this FH capacity it has been considered a more flexible distribution between the RRH and the BBU [2]. It is preferable to preserve some of these blocks in the RRH as opposed to shifting the entire baseband processing to the BBU. Functional splits is the term given to this concept [3]. The three components of the C-RAN are the remote unit (RU), distributed unit (DU), and central unit (CU). The lower physical (PHY) layer functions are hosted by the RU, whilst higher PHY layer functions, medium access control (MAC) operation, and radio control function are carried out by the DU. A CU carries out the higher-level radio access network (RAN) tasks related to the packet data convergence protocol (PDCP) and radio resource control (RRC) protocols for packet data convergence [4]. While DUs are often situated higher in the network to conduct coordination of radio resource allocation and carry out significant operations (radio scheduling, channel coding), the positioning of RUs is as near to antennas as feasible [4]. The functional splits that a mobile network can provide for each next generation Node B (gNB) base stations (BS) relies on the users traffic characteristics and the FH network restrictions. For each gNB in the C-RAN, the best functional split is determined using just given characteristics of the anticipated user traffic, such as the peak or average data rate. This strategy basically dismisses the volatility of user traffic, which is the majority of FH traffic within functional splits [5]. The 3rd Generation Partnership Project (3GPP) proposed eight alternative solutions for the functional splits [6], which will be fully described in this work.
Delivering high-speed data services in densely populated areas may be quite difficult, especially when there is significant signal penetration loss and strong interference. This makes the macrocell deployment inadequate and motivates seeking for alternatives. The adoption of low-power nodes with a smaller coverage range may solve this issue for outdoor users while femtocells are the indoor counterpart.
The utilization of millimeter wavebands (mmW), massive multiple-input multiple-output

(mMIMO) and beyond is a viable alternative for coverage improvement in the fifth generation (5G) of mobile communication technology and beyond, and recent research on channel and radio propagation modeling has been taken special importance [7].
In indoor picocellular environments, the majority of the research that were presented in the literature analyzed the performance of small cellular networks and generally had taken into account optimization theory and single-slope path loss model (SS-PLM) [8]. Analyzing standard path loss models (PLM) is straightforward. Yet, they take into account the single path loss exponent. However, particularly in dense networks, SS-PLMs restricts the accuracy [9]. Alternatively, a two-slope PLM (TS-PLM) is the preferred approach in ultra-dense networks.
The study presented in this master dissertation is motivated by this framework, while considering the two-slope model, proposed in [10] in an outdoor pico cellular scenario, while taking a 5G New Radio (5G NR) deployment to analyze fairness, load balancing, interference management strategies and overall performance of small cell networks, while comparing the cost/revenue trade-off of small cell networks among different frequency bands, for instance functional split 6 and split 7.2.

1.2 Evolution of Mobile Wireless Communication Networks

The data traffic, the number of user equipments (UE), the diversity of applications, and the flexibility of service situations have all increased exponentially in recent years. The evolution of mobile communication technologies over the years has left expectations for improved network performance in each new generation.
According to [11], due to the continued rise in smartphone use, mobile broadband (MBB), and the digitalization of the society and industries, globally mobile network data traffic has doubled in the past two years. The average monthly consumption per smartphone is anticipated to reach 15 GB by the end of 2022 and increase to 40 GB by the end of 2027. Figure 1.1 shows the total global monthly network data traffic from the first quarter (Q1) of 2015 until the Q1 of 2022, and the respective year by year percentage change of mobile data traffic.
The first mobile network generation (1G), offered the first wireless analogue voice services. The second mobile network generation (2G) switched from analog to digital technology and also implemented SMS messaging. The third mobile network generation (3G) introduced the internet access and the first multimedia services, including email and video calling. The fourth mobile network generation (4G) also known as Long Term Evolution (LTE), supports data flow at higher speed than 2G and 3G networks, as well as improved spectrum efficiency (more devices connected without affecting the network) and much lower latency, compared to prior generations.
The 5G of mobile communication technology is meant to deliver larger capacity and enhanced data rates than the previous generation (LTE). 5G is a fast, secure, and reliable linked ecosystem encompassing humans and machines, which allows seamless mobility, efficient connectivity, higher connection density, enhanced industrial productivity, automation, and sustainability [12]. As a result, in order to satisfy demands for increased network capacity, higher user throughput, more effective spectrum utilization, wider bandwidths, lower

Figure 1.1: Total global monthly network data traffic from Q1 of 2015 to Q1 of 2022, along with the year-on-year percentage change. Extracted from [11].

latency, lower power consumption, more reliability, increased connection density, and increased mobility, it is constantly necessary to push the operating range of wireless systems to new limits [12]. An all-connected world of people and things will be possible because of ultra-reliable low latency communications (URLLC) and massive machine type communications (mMTC) [13].

1.3 3rd Generation Partnership Project

The 3GPP addresses radio access, core transport networks, and service capabilities in cellular telecommunications networks [14]. This project consists of three technical specifications (TS) groups: RAN, Services and Systems Aspects, and CN and Terminals. Telecommunications organizations that collaborate in the development of standards and specifications for the underlying technologies (ARIB, ATIS, CCSA, ETSI, TSDSI, TTA, TTC) are involved.
The Release 15 of the 3GPP refers to the initial phase of 5G [15]. It is focused on enhanced mobile broadband (eMBB) services and worked on the basic essential blocks of the new 5G system, detailing the new 5G system access component, also known as 5G NR, and the new 5G CN [16]. This release defined two operation modes for the new 5G architecture, as follows [17]:

- **5G Non-Standalone (NSA) mode** - It allows operators to deliver 5G services in less time and at a smaller cost by leveraging existing LTE radio access and CN infrastructure.

- **5G Standalone (SA) mode** - A brand-new 5G Packet Core will be presented, with various additional features embedded straight in. 5G NR and 5G CN make up the SA architecture. The 5G SA Packet Core architecture will include network slicing (NS), virtualization, ultra-low latency, as well as other features.

The 5G second phase, as defined by 3GPP Release 16 [18], was completed on July 3, 2020, and adds the remaining functionalities, i.e. mMTC and URLLC, to improve performance and comply with the strict requirements of International Mobile Telecommunications 2020 (IMT-2020), as defined by the radio section of the International Telecommunication Union (ITU) [19]. The advantage of mMTC is the ability to handle a large number of Internet of Things (IoT) devices interacting simultaneously, which is the foundation for the new linked society idea. URLLC, on the other hand, offers exceptionally low latency and excellent service availability to meet the unique requirements of vital communications [19]. The second phase of 5G is already capable of dynamically delivering a functional and high performance foundation for highly sophisticated service types employing a range of use cases. This is accomplished via NS, which is included in Release 16 [19]. LTE and 5G NR have several shared components in NR Phase 1. There are two versions: one that uses the LTE core and another that uses an NR core and is entirely independent of the LTE core network [20].

The Release 17 content was approved in December 2019. However it would be then released June 2022, assuming that no more delays would happen [21]. Meanwhile, 3GPP is producing the ”Release 17 Description; Summary of Rel-17 Work Items” [22] with the Work plan manager adding summary notes for each of the features within. Existing features include multiple input multiple output (MIMO), dynamic spectrum sharing (DSS), UE power saving, coverage, positioning, and URLLC, they have been enhanced in Release 17 [23]. Support for reduced capability (RedCap) UEs, operating in frequency bands beyond 52 GHz, multicast and broadcast service (MBS), and non-terrestrial networks (NTNs) are among the major new use cases and deployment scenarios covered in Release 17 [23].

Meanwhile, the content of the next Release 18 was approved, as seen in the figure 1.2, and it is expected to be completed in March 2024 [24]. Release 18 contains 27 different research or development items that will improve network performance and meet new use cases. Work on embracing artificial intelligence (AI) and machine learning (ML) technologies in the evolution of 5G Advanced is highlighted in this Release [23].

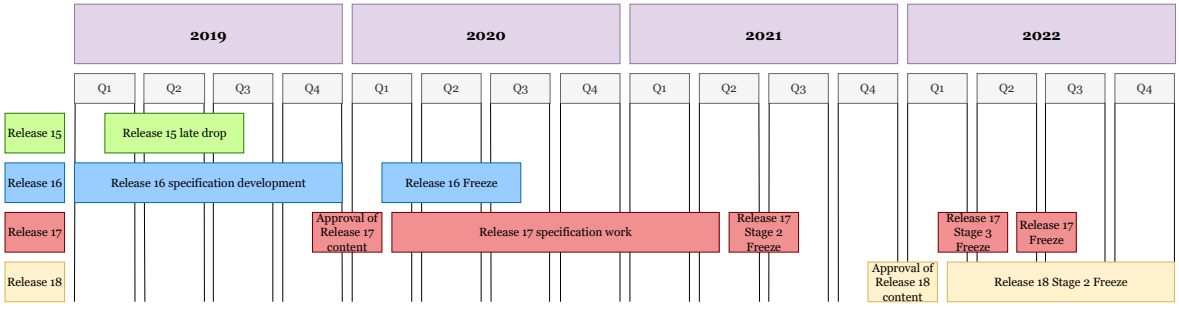

Figure 1.2: Timeline of 3GPP 5G Releases from Q1 of 2019 to Q4 of 2022. Adapted from [15] [18] [21] [24].

1.4 Heterogeneous Networks

Heterogeneous networks (HetNets) are made up of homogeneous cellular macro BSs with high transmission power that are overlaid (or underlaid) with low-power base stations. Picocells, femtocells, microcells, and relay nodes are examples of low-power base stations, which are referred to as small cells [25]. MBB network installations range from densely populated urban areas to remote rural regions, and they operate across a wide spectrum of carrier frequencies with diverse propagation characteristics and coverage levels [26]. HetNets are designed to overcome and improve capacity limitations, as well as network signal coverage and energy efficiency [27]. In figure 1.3, we can observe different types of small cells and macro cells in the different areas that they operate.

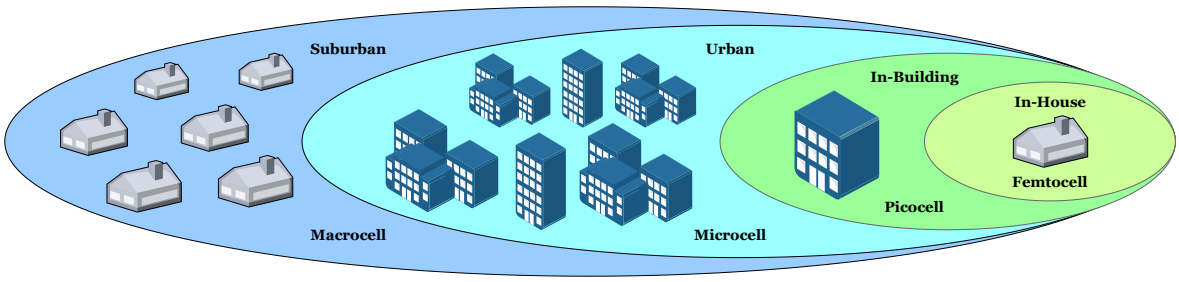

Figure 1.3: Different areas of the small cells and macro cells. Adapted from [28].

The types of cells can be defined as follows [29]:

- **Macrocells** - These cells are the BSs that cover a vast region with an Inter Site Distance (ISD) ranging from a few hundred meters to several kilometers, depending on the density. They provide baseline coverage for any LTE network, ensuring continuous connectivity and uptime. The power usage ranges from 100 W to 450 W, and the antennas are usually divided into sectors that span 120 degrees each [30].

- **Microcells** - These are also known as micro BSs or serving microcells, and they typically have the same interface as a standard BS but broadcast at a considerably lower power. They are normally deployed by an operator, and one of their most popular uses is to act as outdoor hotspots, with coverage typically restricted to 1 mile and regulated by transmit power [31].

- **Picocells** - These are similar to Evolved Node Bs (eNBs), with the exception that they have a lower transmit power than macrocells. They are usually equipped with omnidirectional antennas (not sectorized) and positioned in a planned (hot-spot) way indoors or outdoors [29].

- **Femtocells** - These are consumer-installed (unplanned) network nodes for indoor use, with network BH provided via the consumers home digital subscriber line (DSL) or cable modem [29].

1.5 Objectives and Approach

This MSc dissertation proposes the study of achievable system capacity when a numerology zero is considered, for three frequency bands (2.6 GHz, 3.5 GHz, and 5.62 GHz). This work address 5G NR for an urban micro (UMi) cell scenario, where the frequency range is between 0.5 and 7 GHz, and it is defined as the model A. In order to determine radio and network performance, the urban micro scenario model (UMi_A) was implemented in the 5G-air-simulator. It is possible to determine the saturation level by determining the number of users corresponding to the results for the packet loss ratio (PLR) lower than 2% [32]. Another objective of this dissertation is to study the performance of two schedulers, in terms of quality-of-service (QoS). The QoS-aware modified largest weighted delay first (M-LWDF) scheduler and the QoS-unaware proportional fair (PF) scheduler have been considered. The different techniques have been evaluated by using an urban micro scenario. We first analyzed the PLR for M-LWDF and PF schedulers, while studying the impact of break point distance for different frequency bands. By deploying the 19 cells, the simulation setup is first established. These findings are used to analyze the goodput, the number of supported users, and PLR for three frequency bands. Then, with consideration of goodput, an amount of supported users, and PLR, the costs/revenues and profit have also been estimated for the PF and M-LWDF schedulers, by considering video (VID) and video plus best effort (VID+BE) traffic, with or without consideration of the functional splits (7.2 and 6), for the three considered sub-6 GHz frequency bands.

1.6 Contributions

The main contribution of this dissertation was the comparison of the cost/revenue trade-off of small cell networks among different frequency bands, for functional split 6 and split 7.2. The work associated with this dissertation is based on research on 5G NR for a UMi cell scenario of HetNets while analysing fairness, load balancing and interference management strategies, and overall performance of small cell networks.

1.7 Outline of the Dissertation

The first part of this master dissertation gave a brief introduction about the evolution of mobile wireless communication networks, the 3rd Generation Partnership Project and contributions of its technical releases to the standardization of mobile technologies and HetNets.
In chapter 2, the state of the art is presented, and the rearrangement of the RAN is discussed by introducing the C-RAN, the utilization of common public radio interface (CPRI) and enhanced common public radio interface (eCPRI), the introduction of functional splits, as well as Open RAN (O-RAN). It also covers topics such as HetNets, Frequency Ranges and Propagation Model. The Path Loss Model and the Supported Throughput formulation used in the work of this dissertation is also addressed.
Chapter 3 presents the considered radio and simulation parameters that are considered to

evaluate the system performance, as well as the results at the saturation level, in terms of PLR, delay, goodput and fairness, and the results for the maximum network performance. It also specifies the equations and parameters needed to calculate costs, revenues, profits, and other variables, analyzing the impact of applying or not the functional splits.
Finally, chapter 4 draws conclusions the the work, with a brief overview of the obtained results followed by suggestions for future work.

Chapter 2

State of the Art and General Concepts

2.1 Introduction

The goal of the 5G of mobile communication technologies is to provide an extensive and superior mobile service. It should benefit a variety of industries, including those related to transportation, manufacturing, healthcare, energy, public safety, and agriculture. In the next years, it is anticipated that the number of users, traffic volume, and data rate would all rise [33]. Solutions are thus required to satisfy the needs of both mobile consumers and business. Rearranging the network's architectural layout, namely through redesigning the RAN, is one of the more appealing choices. In order to reduce traffic growth, build cost-effective networks, and provide enhanced QoS to large end-user populations, several designs and technologies for the Fifth Generation of mobile networks, notably in RAN, have been proposed [34].

2.2 5G RAN System Architecture

The RAN is a part of a mobile telecommunications network that uses radio access technology (RAT) to connect UE to the CN. This technology will also be used to exchange data with mobile devices over the air interface [35].
Since the introduction of the 2G of mobile communication systems, the RAN design has been constructed by using monolithic building blocks. These networks, as well as certain 5G networks, contained BBUs, which interpret and modulate radio frequency (RF) signals at the base of radio towers, turning the output into digital data that is then sent in the BH to the CN [36]. Figure 2.1 shows the distributed RAN (D-RAN), where the link between the BBUs and the CN is known as the BH network, while the connection between the BBUs and remote radio units (RRU) is known as the FH network [37]. Since the RRUs and BBUs are directly linked through CPRI, there will be one BBU connected to analyze data for each RRU.
The China Mobile Research Institute (CMRI) came up with the idea of C-RAN. C-RAN may gain significantly from improvements in energy efficiency, capital expenditure (CAPEX), operational expenditure (OPEX), capacity, and traffic offloading [38]. By consolidating the processing of BBUs, the energy consumption of air conditioning and other support equipment can be significantly reduced. Figure 2.2 shows the C-RAN architecture. The FH network, which connects the BBU and RRHs, is an eCPRI or wireless link with low latency and high capacity. The pooling of BBUs provides centralized management and operation, which results in considerable reduced costs in the rental of BSs, as well as in operation and maintenance. The C-RAN architecture can be used to deploy more sophisticated transmit and receive wireless communications technologies, resulting in significant network capacity gains. When it

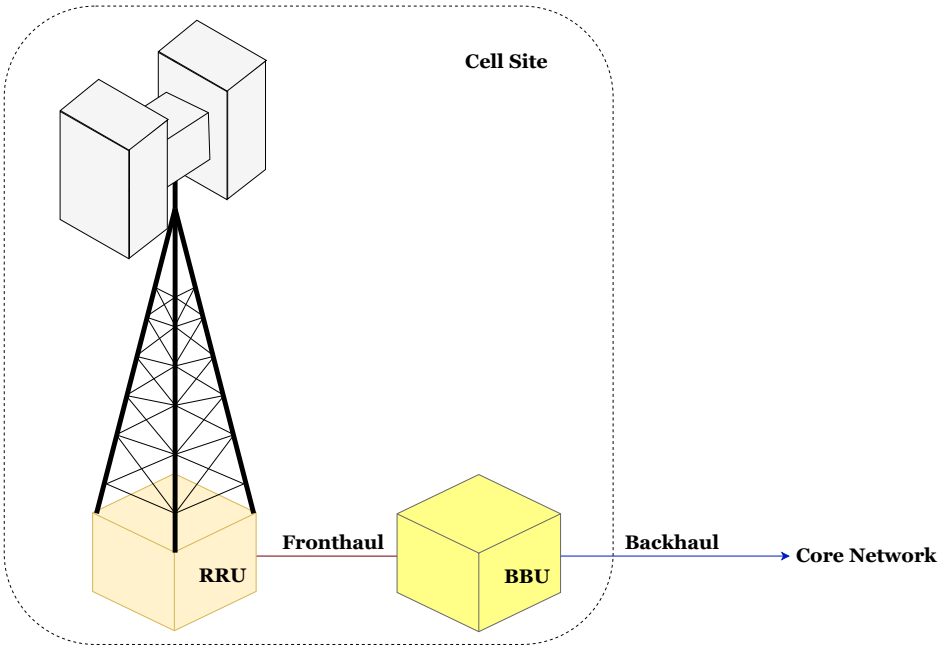

Figure 2.1: D-RAN Architecture, that consists of the link (fronthaul) between the RRU and the BBU inside the cell site, and the connection (backhaul) between the BBU and the Core Network.

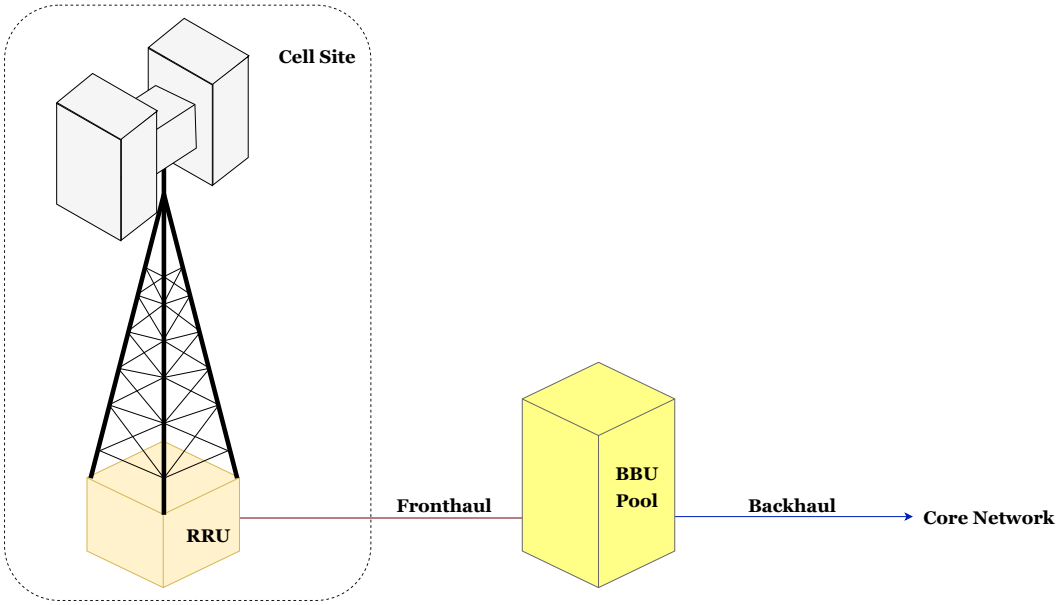

Figure 2.2: C-RAN Architecture, formed by the RRU inside the cell site with the link (fronthaul) to the BBU pool, which is then connected (backhaul) to the Core Network.

is possible, BBU pooling can act as a transition point for traffic offloading from the CN to other network connection points, and radio access technologies [38].

The CU, DU, and RU, which are each capable of hosting a distinct function of the 5G NR, are the three logical nodes that make up the new flexible architecture for the 5G RAN that was established by the 3GPP. Performance metrics like latency and cost can be coordinated due to the use of a split architecture (between CU and DU). Based on the services they provide and the economics of the available transportation networks, operators must determine the appropriate functional split. Telecom equipment makers must choose the finest alternative for their target customers. There is no functional split that will work alone in all situations [39].

2.3 Common Public Radio Interface and Enhanced Common Public Radio Interface

LTE FH connections often utilize the CPRI connection protocol. CPRI establishes a basic digital interface standard between the Radio Equipment Control (REC) and Radio Equipment (RE) of the radio BSs [37]. The user plane data, control and management Plane, and synchronization plane are the three data flows that make up the CPRI protocol. These flows are specified at the PHY layer (layer 1) and data-link layer (layer 2) levels [40]. User plane carries in-phase and quadrature (IQ) data, control planes transmit and receive control signals from distant radios, while sync planes keep baseband and remote radio units in sync [41]. An electrical interface (such as what is found in conventional radio BSs), and an optical interface, are supported by layer 1 (for radio BSs with remote RE). Scalability and flexibility are supported by layer 2 [40].

Although chained topologies are supported, the primary application of CPRI is as a point-to-point interface that demands a direct connection between the RE and REC, having assigned the REC role for the master port and the RE role for the slave port. The fundamental design of the CPRI is shown in figure 2.3 [40]. The most recent CPRI specification allows for line rates of up to 24.33 Gbps (CPRI Rate 10) [40]. Considering that CPRI is a constant bit rate protocol, the transmission line must maintain the selected bit rate regardless of the actual data flow in the radio cell. This has obvious efficiency problems with 5G, as FH data rates are projected to exceed several hundreds of Gbps [42]. As a solution, the eCPRI protocol was established. By supporting Ethernet-switched or IP-routed FH networks, the major goals of eCPRI are to reduce the amount of transport network bandwidth required and to increase flexibility and reliability in the placement of the functional split. As shown in figure 2.4, the FH transport network links the eCPRI Radio Equipment Control (eREC) with the eCPRI Radio Equipment (eRE). The interworking function (IWF) was developed to act as a bridge between eCPRI and CPRI nodes, enabling the eCPRI to operate alongside CPRI devices. Vendor-specific information that depends on the functional split selected is delivered through eCPRI [43].

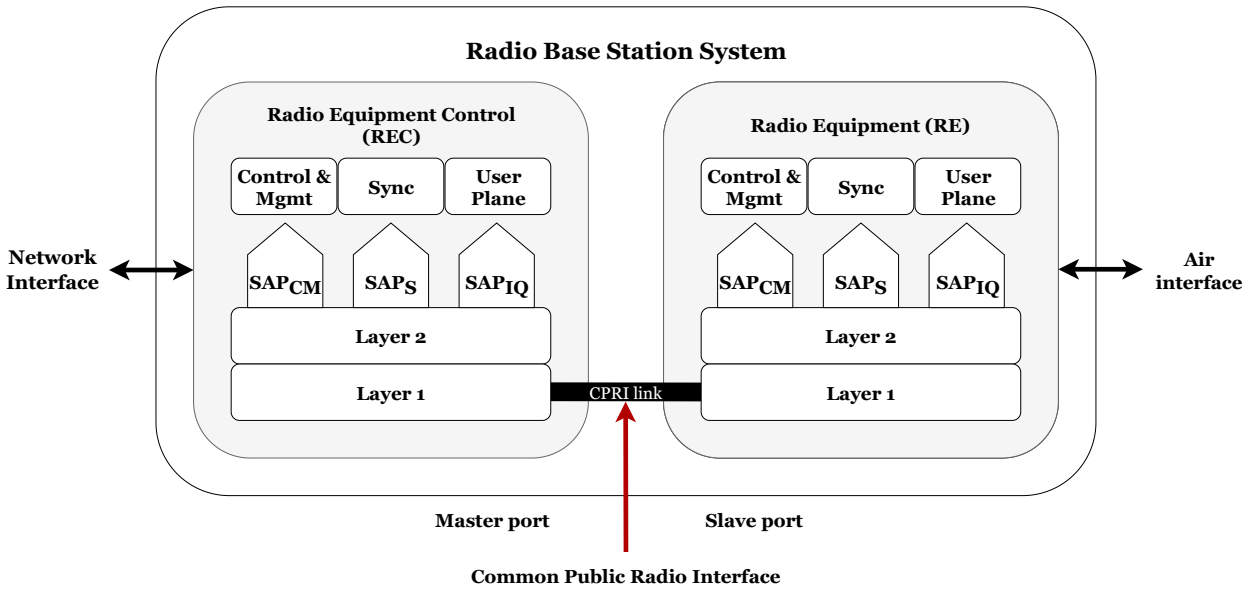

Figure 2.3: Basic architecture of a CPRI based RAN, in which there is a connection between the RE and the REC. Adapted from [40].

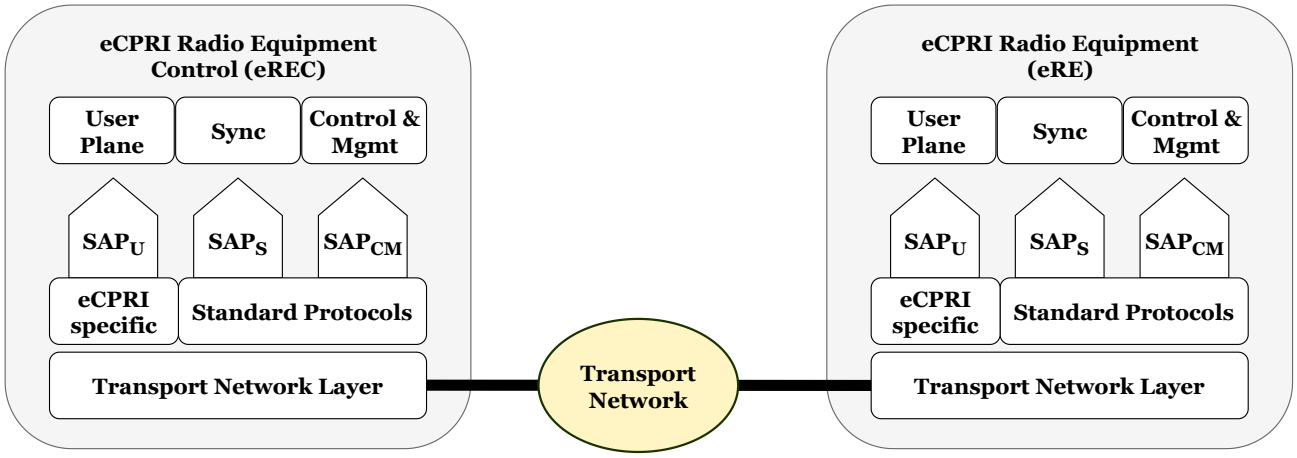

Figure 2.4: Basic eCPRI structure, which presents a link, through the fronthaul, between the eREC and the eRE. Adapted from [43].

2.4 Functional Splits

Given the advantages of C-RAN, a mobile network operator should attempt to centralize as many functions as feasible. To manage the same amount of user traffic, more FH capacity is required as more functions are centralized. As a consequence, the characteristics of user traffic as well as the limitations of the FH influence the functional split that a mobile network is able to obtain, for each gNB [5]. The selection of the functional split for the implementation phase is a major focus of the current study on this subject. In other words, only a priori characteristics of the designed user traffic, such as the peak or average data rate, are utilized to determine the appropriate functional split, for each gNB in the RAN. This method effectively ignores user traffic volatility, which represents a significant portion of FH traffic, for the majority of functional splits [5].
Eight functional split alternatives with corresponding sub-options were presented by the 3GPP. As they will be situated at the antenna mast, the remaining functions in the DU are relatively near to the users, while those in the CU will gain from processing centralization and high processing powers inside a datacenter [44]. As seen in the figure 2.5, the red arrows depict several alternatives for functional splits, the functions to the left of the red arrow are implemented in the CU, while the functions to the right of the red arrow are performed in the DU.

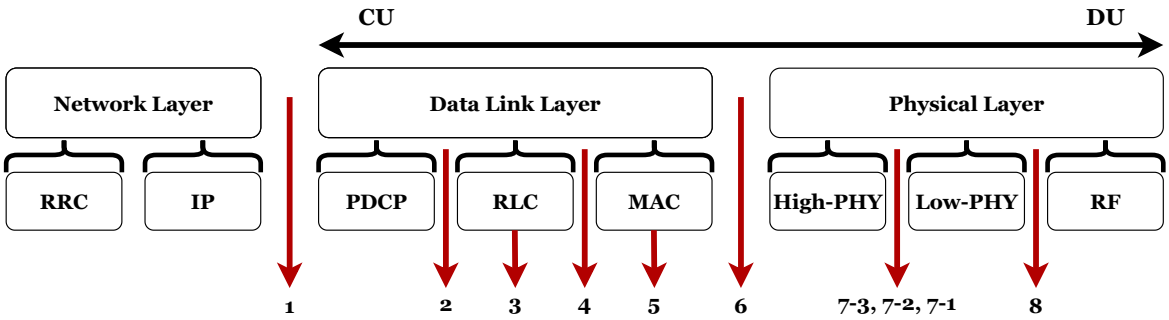

Figure 2.5: Different functional splits proposed by 3GPP. Adapted from [6].

According to [45], the most popular splits that have been defined are: **option 7**, usually referred to as intra-PHY layer functional split, puts several radio capabilities at the RRHs, including inverse fast fourier transform (IFFT), cyclic prefix addition, resource mapping, and precoding functions; **option 6** that transfers all RF and PHY layer operations to the RRH, also known as the MAC-PHY split; and **option 2** the split of the PDCP and the radio link control (RLC), also known as PDCP-RLC split.
A few similar splits with the names E, I_U, I_D, II_D and D have recently been added to the eCPRI specification [43]. Splits I_U, I_D, II_D are found in the PHY layer and thus correspond to option 7. Split E, on the other hand, relates to option 8 and is identical to the standard split used by CPRI, while split D refers to option 6 and below, as described in [45].
The downlink (DL) and uplink (UL) FH bit rates for the various functional splits are shown in figure 2.6. The computations were performed on an LTE network, however the results still apply to 5G NR. The graph demonstrates that the FH bit rates are higher for the low-level split choices, 7 and 8, and then considerably decrease for higher level splits while being

reasonably constant for options 1 to 5 [44]. The PHY-level functional splits, often known as Option 7, are quite popular in the industry. Option 7 provides a nice combination between FH bandwidth, RU complexity, and inter-cell collaboration [39].

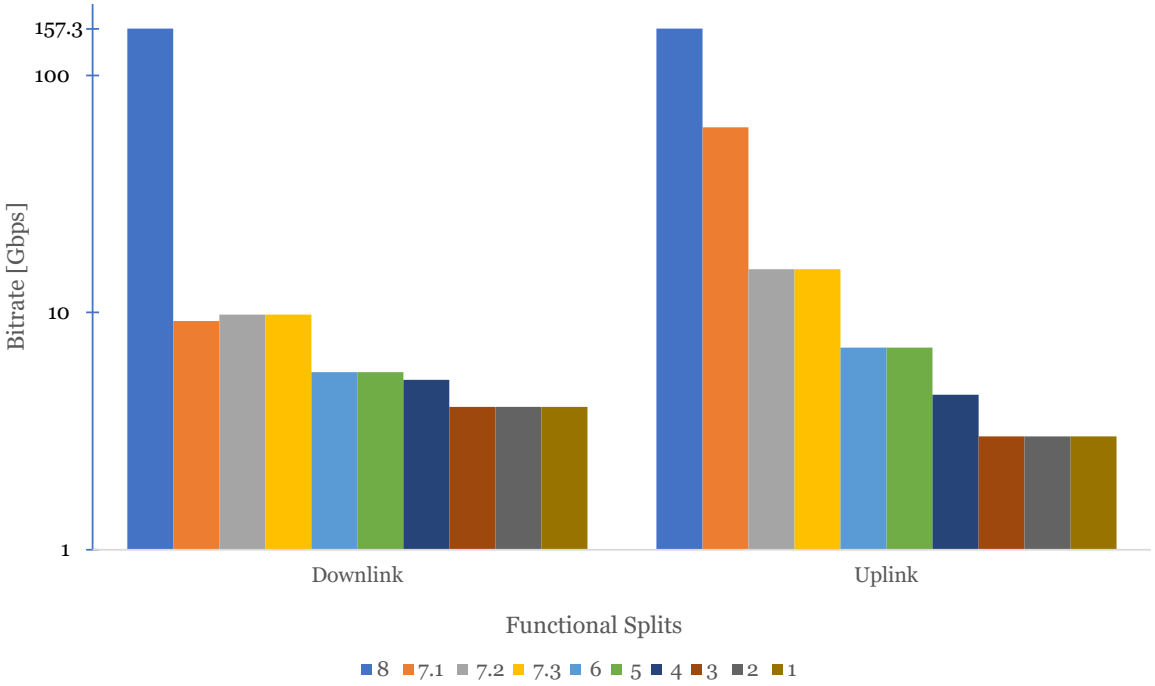

Figure 2.6: Fronthaul bit rates for each functional split option in UL and DL. Adapted from [44].

2.4.1 RF-PHY Split (option 8)

The 3GPP RF-PHY specified split was already taken into consideration in classic C-RAN based design, including CPRI supported RRUs, but it still has significance in certain particular 5G business applications [46]. To achieve maximal virtualization benefits, this split allows total separation of the RF from the PHY layers. A tightly coordinated RAN is the consequence of everything being centralized, from the PHY layer and up, including all protocol layer levels [46]. Due to the concentration of operations at all protocol layer levels made possible by this split, the RAN is tightly coordinated. This enables to successfully handle coordinated multi-point transmission and reception (CoMP), MIMO, load balancing, and mobility [6]. Since the automatic repeat request (ARQ) is centered in the CU, this approach may be more durable under non-ideal transmission circumstances and during mobility [6]. CPRI is a time division multiplexing-based constant bit rate FH interface since it conducts the framing at regular intervals. This protocol was created exclusively for the transfer of radio waveform samples [44]. Split option 8 has a FH connection bit rate that scales with the number of antennas but is continuous, extremely high, and does not scale well for huge MIMO situations [44].
The DU and RU should be able to communicate with other DUs and RUs from external parties. The improvement over the traditional split 8 is that RUs must now use eCPRI instead of the conventional CPRI interface between the RU and the DU if they want to operate var-

ious technologies over the same FH interface. This strategy provides centralized traffic aggregation from the RUs, allowing for a smooth transition from the standard LTE to the NR environment [36].
The latency of the functional split option between PHY and RF is 250 μs after careful evaluation and examination of numerous vendors equipment specs and implementation methods [47].

2.4.2 Intra PHY Split (option 7)

The PHY layer is in charge of converting digital bits into outgoing radio waves, in the DL direction, and the opposite, in the UL direction [44]. The number of users that are in the current cell determines the FH bit rates for the functional splits in the PHY layer [44].
It is possible to significantly relax the FH requirements in terms of both bandwidth and latency by locating some PHY layer functionalities such as Fast Fourier transform (FFT) or IFFT, subcarrier mapping/demapping, signal equalization, and MIMO processing at the DUs [48]. In this case the CU contains the whole protocol stack as well as the remaining PHY components.
Option 7 is decomposed into sub-options 7.1, 7.2, and 7.3. The PHY layer of the stack is differently divided by these three sub-options of functional split option 7, between the DU and the CU. The primary difference between the level 7 splits is the data rates on the FH network. However, they all support the fundamental advantages of centralization, such as carrier aggregation, MIMO, and CoMP [39]. The FH bit rate is greatly decreased by all three alternatives since the FFT capability is left in the RU. Pre-coding and resource element mapping are two additional functions that are given to the RU in option 7.2, which significantly lowers the FH bit rate compared to option 7.1 [39]. Locating this function in the RU results in a fluctuating bit rate on the FH network because the resource element mapping identifies unused subcarriers from the RF link. The option 7.1 provides a consistent bit rate. Option 7.3, which only affects the DL, significantly reduces the FH bit rate by giving the RU additional responsibilities, making it more complex [39]. For relatively straightforward RU designs, all three splits provide a decent balance between the demands of FH and centralization. These choices become contenders for high-capacity networks in crowded urban environments. With its lower and varied FH bit rate, and is compatible with the eCPRI protocol. Option 7.2 has, nonetheless, acquired more and more support within the industry [39].

2.4.3 MAC-PHY Split (option 6)

The data link layer and the PHY layer are separated by split option 6. The MAC scheduler is centralized, and all PHY processing is done locally [44]. The FH content is transport blocks, which significantly decreases the FH link bandwidth, and the centralized CU pooling gain offers effective resource management and optimization. With this split, the Ethernet frame, scheduling management, and synchronization will all add additional cost to the FH bit rate [46]. The hybrid automatic repeat request (HARQ) and other time-critical procedures are concentrated in the CU-pool, therefore option 6 has extremely severe delay requirements

[44]. In the MAC/PHY split, the reference [49] depicts the one-way latencies as optimal or near-ideal. The advantages of shorter subframes and broader channel bandwidth may be decreased by any FH delays, however these benefits are stronger in circumstances of non-ideal transmission conditions and during mobility since the ARQ is centralized in the CU [44]. Due to the separation of the PHY layer and the MAC in this split option, an in-band protocol is required to provide modulation, multi-antenna processing, and physical resource block (PRB) allocation [46].

2.4.4 Intra MAC Split (option 5)

The MAC sublayer is divided into high and low MAC sublayers by this split. Multiple Low-MAC sublayers will be managed via centralized scheduling in the High-MAC sublayer [6]. The Low-MAC sublayers time-critical functions include those with strict delay requirements (such as HARQ) or those whose performance is proportional with latency (e.g. radio channel and signal measurements from PHY, random access control), shortening the FH interface delay requirements [6].

2.4.5 RLC-MAC Split (option 4)

In this this split, MAC service data units (SDUs) are sent in the UL direction while RLC protocol data units (PDUs) are received in the DL direction [44].
In [50], since 5G air interface subframe sizes are smaller than those of LTE, a functional split between RLC and MAC layers may therefore be impossible. Particularly, shorter subframe sizes enable the scheduler to make choices more frequently, better adjusting to traffic needs or channel circumstances. Nevertheless, this results in more frequent signal transmitted to the RLC from the MAC, defining the size of the next group of RLC PDUs [44].
According to the studies made in [51] on the effect of FH latency on the RLC ARQ protocols, all ARQ protocols throughput is seen to be severely reduced by the delay imposed by the FH network.

2.4.6 Intra RLC Split (option 3)

The RLC is divided into two categories in this split: low RLC and high RLC. Additionally, two strategies based on real-time and non-real-time functional splits are taken into account [6]:

- **Option 3.1** - The high RLC is made up of ARQ and other RLC functions, whereas the low RLC is made up of segmentation functions [44]. The FH latency restrictions are minimized by this option since real-time scheduling is done locally in the DU. Since the ARQ is centered in the CU, this option could be more durable under non-ideal transmission circumstances and during mobility [6]. In [52], the 3GPP defines the DL FH bit rate for split option 3 as being lower than option 2.
- **Option 3.2** - The sending entities make up the low RLC, whereas the receiving entities make up the high RLC [6]. This option does not take into account the transmission network delay between the CU and DU and places the flow control in the CU [6].

2.4.7 PDCP-RLC Split (option 2)

While the other functions are carried out locally in the DU, the PDCP and RRC are centrally managed. This split makes it easier for components to interact with one another by using a pre-existing standardized interface [49]. This split supports multi-connectivity and does so by breaking up traffic into many flows that may be sent to various access nodes [53]. The benefits of this functional separation include centralized over-the-air encryption, increased possibility for mobility coordination, and easier handover operations, such as data forwarding from the old serving cell to a new serving cell in a CU containing BSs functions above RLC layer [50]. The PDCP-RLC still depends on the DU to execute the same computationally demanding MAC and PHY layers, even if it lacks sufficient centralized functions to conduct any type of sophisticated coordination mechanism with other gNBs [5].

2.4.8 RRC-PDCP Split (option 1)

In this split option, the RRC layer is situated in the CU, while the other levels of the protocol stack are located in the DU [6]. This approach allows for both centralized control plane and distributed user plane deployments by separating the control plane (i.e., RRC) from the user plane [54]. This split could not be advantageous for implementations where several cells are linked to a CU-pool since, according to [43], it will not enable a variety of functions, including those that provide inter-cell coordination. The user will still gain from quicker mobility management thanks to the RRC centralization since many functions are conducted locally [49]. Furthermore, having a centralized RRC allows one or more service applications to get network information [49].

2.5 Open RAN

Mobile network operators and network equipment providers recognized the need for a flexible and open approach in RAN development throughout the previous decade, which has since been termed O-RAN. In 2018, two alliances, the xRAN forum and the C-RAN forum, merged to create this approach. This strategy intends to make multi-vendor mobile radio access network implementation and integration easier, as well as removing potential roadblocks in future improvement. It also plans to make RAN more intelligent and flexible through supporting the cloud-RAN idea and through implementation of ML and AI [55].

2.5.1 Split Option 7.2x

Split Option 7.2x, a new feature in the O-RAN FH specifications for functional splitting, inserts some Layer 1 functions normally situated in the baseband processing section, in the radio equipment. It also includes Management Plane standards, as well as Control, User, and Synchronization Plane specifications that, while sticking to the eCPRI architecture, dictate precise signal formats and equipment operation necessary for multivendor RAN not covered by the eCPRI specifications [56].

The split option 7 has three subvariants, as seen in section 2.4.2. O-RAN chooses split 7.2x, in which the bandwidth requirement is proportional to the number of spatial layers, while in splits 7.1 and 7.3 the bandwidth requirements are proportional to the number of antenna elements and coded bits, respectively [57]. Split 7.2x is divided into two groups by O-RAN: Category A and Category B. They differ in where the decoding function is placed, with Category A in DU and Category B in RU, with the second supporting more complicated MIMO configurations [56].

2.5.2 O-RAN Architecture

The O-RAN reference architecture is intended to support next-generation RAN. The architecture is built on well-defined, standardized interfaces to provide an open, compatible supply chain ecosystem that supports and complements 3GPP and other industry standards [58]. Figure 2.7 shows the O-RAN reference architecture. The radio side of the O-RAN architecture contains Near-Real-Time RAN Intelligent Controller (Near-RT RIC), O-RAN Central Unit Control Plane (O-CU-CP), O-RAN Central Unit User Plane (O-CU-UP), O-RAN Distributed Unit (O-DU), and O-RAN Radio Unit (O-RU). On the management side, there is a Non-Real-Time RAN Intelligent Controller (Non-RT RIC) function in the Service Management and Orchestration (SMO) Framework.
The main elements of the O-RAN architecture can be defined as follows:

- **Non-RT RIC** - It is a piece of the SMO in the O-RAN architecture, and it comprises a platform and a series of microservices (designated radio access network automation applications (rAPPs) by the O-RAN Alliance) that reflect the intelligence [59]. Non-RT RIC main objective is to enhance intelligent RAN optimization by providing policy-based assistance, ML model management, and enrichment information to the Near-RT RIC function, allowing the RAN to optimize [60]. The rAPPs are modular applications that use the Non-RT RIC Framework capability to conduct RAN optimization, and other activities [61].

- **Near-RT RIC** - It is a logical function that enables Radio Resource Management (RRM) optimization based on fine-grained data gathering and actions, as perceived by the market. As microservices, Near-RT-RIC runs one or more xApps-dedicated apps (provided also by third parties) [55]. Multiple E2 Nodes, such as O-CU-CPs, O-CU-UPs, O-DUs, and O-RAN Evolved Node B (O-eNB), can be linked to a Near-RT RIC [62].

- **O-CU-CP** - It is a logical node hosting the RRC and the control plane part of the PDCP protocol [61].

- **O-CU-UP** - It is a logical node hosting the user plane part of the PDCP protocol and the Service Data Adaptation Protocol (SDAP) [61].

- **O-DU** - It is a logical node hosting RLC, MAC protocols and High-PHY layer [61].

- **O-RU** - It is a logical node hosting Low-PHY and RF processing [61].

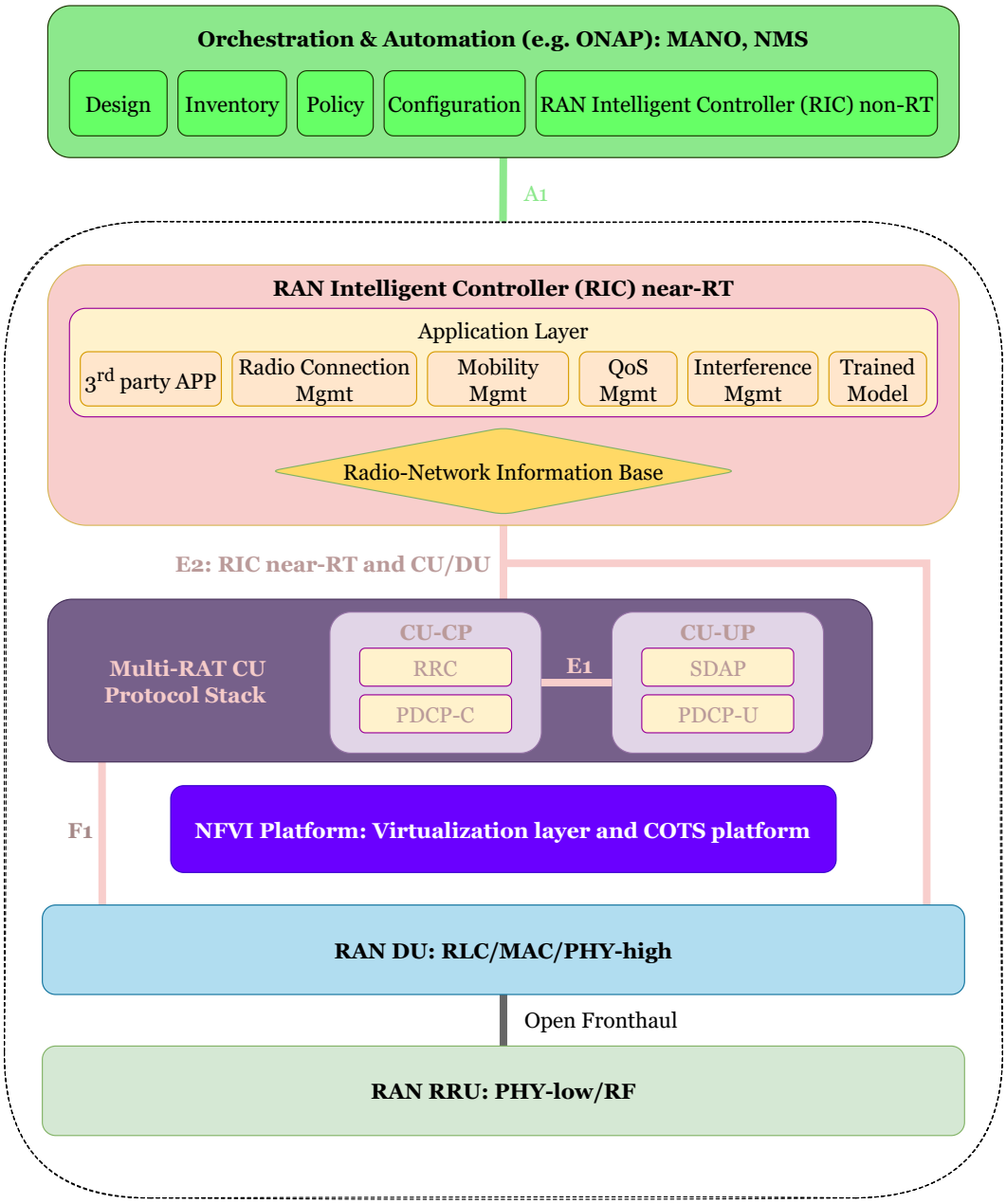

Figure 2.7: O-RAN architecture by ORAN Alliance. Adapted from [58].

2.5.3 Benefits of O-RAN

The O-RAN is a long-awaited technology that industry describes as a solution that provides a set of benefits to both operators and end-users. It is a RAN-specific framework for upgrading commercially-proofed 3GPP solutions by creating new interfaces and nodes from the ground up [55]. By merging software and hardware disaggregations through open interfaces, it specifies new technological solutions and business models to address rising prices, difficult deployments, and other issues [63].
The main benefits of the O-RAN Architecture which are stated in the O-RAN Alliance whitepaper [64], are as follows:

- **Lowering network CAPEX and OPEX** - O-RAN can lower CAPEX by utilizing a thriving multi-vendor ecosystem with scale economics, and is also lowers OPEX by RAN automation.
- **Potential to boost network efficiency and performance** - Through closed-loop control, O-RAN will be able to provide efficient, optimal radio resource management, hence improving network performance and user experience.
- **Ability to quickly add new capabilities** - With its native cloud infrastructures, O-RAN makes it simple to add additional network capability with a simple software upgrade.

2.6 Frequency Ranges

The air interface used in LTE is insufficient for 5G in terms of flexibility and efficiency mainly due to the broad range of use-cases, spanning from very high mobile bandwidth to extremely low latency and vast amounts of connections. The newest radio access technology, 5G NR, was created expressly to meet the needs of 5G. To address LTE limitations, it includes the utilization of additional frequency bands, as well as several architectural improvements.
The most simple technique to boost a communications system's data rate is to expand the radio channel bandwidth. Although it may seem simple, the problem is significantly more complicated since the use of the frequency spectrum is highly regulated to reduce the impact of interference. With regard to the bandwidth requirements of 5G, these frequencies are very congested and have very limited room. As a result, two separate frequency ranges for 5G NR have been specified. According to [65], the frequency range 1 (FR1) contains frequencies from 410 MHz up to 7125 MHz, and frequency range 2 (FR2) ranges from 24250 MHz up to 52600 MHz.
Due to its initial upper limit of 6 GHz, FR1, also known as the "sub-6 GHz" 5G, combines some of the frequency bands utilized in earlier mobile technologies with new, underused bands. Even while FR1 does not provide as much additional spectrum as FR2, such frequency bands suffer reduced radio channel attenuation, which improves cell coverage [66].
The FR2 is also known as 5G mmW bands since it uses millimeter wavelength radio signals. While additional methods are still employed in FR1 frequencies, the major advantage of operating at FR2 is the quantity of spectrum that is accessible, allowing for the utilization of

broader transmission bandwidths. It would be challenging to integrate the 400 MHz maximum carrier bandwidth for FR2 in the FR1 channels in 5G. On the other hand, millimeter waves have greater attenuation and correspond to smaller cell sizes. FR2 cells may be more densely deployed to get around this problem. As a consequence, the stress on the overused lower frequencies may be minimized, and overall network efficiency is increased, by focusing the FR2 deployments into areas where the high data rates are required, such as city centers, while extending the FR1 cells 5G coverage [66].

2.7 Propagation Model

Mobile operators ultimate goal is to provide enough coverage and QoS to their customers. The mobile radio channel has a significant impact on the operation of wireless communication systems. Hence, anticipating the propagation characteristics between the transmitters and receivers is essential for the design and implementation of a radio network communications system. All calculations and simulations rely on accurate propagation models. A propagation model is an equation for describing and forecasting radio wave propagation [67]. The environmental variables, the kind of application, the frequencies to be applied, the distances to be considered, and the computing cost of the chosen model all play a role in selecting a propagation model [31]. Empirical models, semi-empirical (or semi-deterministic) models, deterministic models, and hybrid models are the four most common types of large-scale propagation models [68].
This propagation models can be defined as follows:

- **Empirical Models** - An empirical model is one that is based on measurements and observations. These can be used to investigate general behavior or to estimate the number of cells necessary in a large area. Empirical models are further split into time dispersive and non-time dispersive categories. Time dispersive gives information on the channel's time dispersive features, such as the multipath delay spread. To anticipate average path loss, non-time dispersive models take into account a variety of factors like distance, antenna heights, frequency, and transmitter power [69].

- **Semi-empirical Models** - The broad availability of digital terrain data, such as terrain height, land use information, and building data, motivated the creation of site-specific propagation models and their incorporation into radio planning software. The comprehensive terrain parameters, gathered along the unique propagation paths between transmitter and receiver, are used to create site-specific propagation models [70].

- **Deterministic Models** - Deterministic models are numerical approaches for simulating the propagation of radio waves by simulating the physical propagation processes. To give a realistic and detailed assessment of the route losses and channel parameters, these models require a specified location for the transmitter and receiver [67].

- **Hybrid Models** - For complex cases, two or more propagation models can be integrated into a hybrid model. Hybrid models sometimes include transferring the out-

puts of one propagation model as inputs to another, combining the benefits of distinct propagation models while avoiding their disadvantages [68].

2.8 Path Loss Model

The propagation loss, or the difference in signal strength between a transmitter node and a receiver node, is one of the most important considerations in the cell design process. These losses are brought on by co-channel interference, which is imposed by nodes in the same layer or other sublayers [71].

The framework and overall objectives of the future development of International Mobile Telecommunications (IMT) for 2020 and beyond (IMT-2020), defined in the ITU recommendation ITU-R M.2083, [72], identifies characteristics for IMT-2020 that would make it more efficient, fast, adaptable, and reliable while offering a variety of services in the planned usage scenarios. The report M.2412-0 from the ITU Radiocommunication Sector (ITU-R) [10] specifies procedures, methodologies, and criteria (technical, spectrum, and service) for analyzing the candidate IMT-2020 radio interface technologies (RITs) or sets of RITs (SRITs) for a variety of test environments. This report provides for some degree of freedom in incorporating new technology [10].

To handle the increased complexity in system modulations, a three-dimensional space (3D) channel model is necessary. In figure 2.8, the distances in 3D are defined, where h_{UT} is the antenna height at the user terminal (UT), and h_{BS} is the antenna height at the BS. The distance between the UT and the BS on the horizontal plane, in meters, is defined by d_{2D}. d_{3D} is the 3D distance between the receiver and the transmitter antenna, in meters. The PLM for

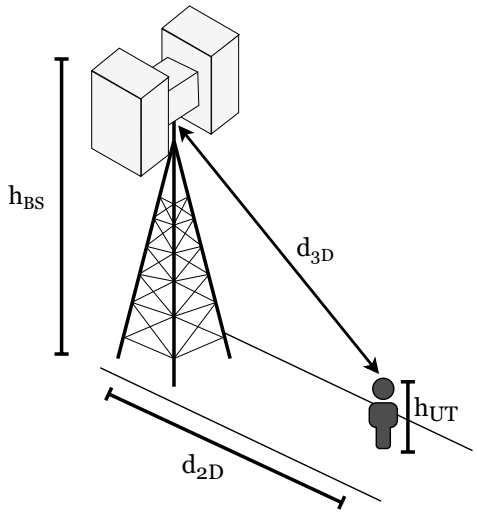

Figure 2.8: Definition of d_{2D} and d_{3D} for outdoor UTs. Adapted from [10].

the UMi Line-of-Sight (LoS) conditions used in the work presented in this dissertation is a deterministic TS-PLM. Since the UMi LoS is applied in the frequency range from 2 GHz to 6 GHz in this case, it was followed the UMi_A LoS scenario defined in [10].

The following equation determines the path loss, PL, between the cell center to the break-

point distance, d'_{BP}:

$$\text{PL}_a = 22.0 \log_{10}(d_{3D}) + 28.0 + 20 \log_{10}(f_c),\ 10\ m < d_{2D} < d'_{BP}, \quad (2.1)$$

where f_c is the center frequency, in Hz.
Equation 2.2 determines the PL, for longer distances than d'_{BP}.

$$\text{PL}_b = 40 \log_{10}(d_{3D}) + 28.0 + 20 \log_{10}(f_c) - 9 \log_{10}((d'_{BP})^2 + (h_{BS} - h_{UT})^2),\ d'_{BP} < d_{2D}. \quad (2.2)$$

The BS and the UT antennas are placed outdoor and located below the rooftops of surrounding buildings. The break point distance, d'_{BP}, is calculated as follows:

$$d'_{BP} = \frac{4(h_{BS} - h_E)(h_{UT} - h_E)f_c}{c}, \quad (2.3)$$

where h_{BS} is the antenna height for the BS, h_{UT} is the antenna height for the UT, h_E is the effective environment height, c $= 3.0 \times 10^8$ m/s is, typically, the propagation velocity of a signal in free space, and h_E is the effective environment height, for UMi_A is equal to one.
For the penetration loss according to [10], it was took into account the average penetration loss, μ, which is 9 dB, and its standard deviation, σ_P, which is 5 dB. According to table 2.1, the LoS probability is defined as being equal to one. Shadowing, which is modeled by a random

Table 2.1: Radio and simulation parameters for UMi_A

UMi_A	
μ [dB]	9
σ_P [dB]	5
LoS probability	1
Shadowing fading standard deviation [dB]	3
Shadowing correlation distance [m]	10

variable, is the attenuation of signals caused by objects placed between the transmitter and reception nodes. The path loss will be the same at equal distances if just equation 2.1 and 2.2 are considered, ignoring shadow fading.
The standard deviation for the shadow fading, σ_{SF}, is represented as a log-normal variable in [10]. In UMi_A for the LoS, the σ_{SF} is equal to 3 dB. The shadowing correlation distance, which for the UMi_A is considered to be 10 m, models the shadowing variable between the BS and the moving UT [73].

2.9 Supported Throughput Formulation

UL and DL often refer to the same thing, even though they have several uses. UL is refered to the direction of communications from a device to the network core, and on the other hand, DL is the direction of communications from the network core to a device. Sidelink (SL), however, uses a direct and proximity-based cellular connection. Since it occurs between two devices, it is referred to as direct. Because the two devices must be in close proximity to one

another, it is considered proximity-based [74]. The calculation of the DL, UL, and SL max data rate supported by the UE is preceded by the band or combination of bands supported by the UE by taking Release 16 of the 3GPP TS 38.306 into account, and keeping in mind the 5G NR assumptions.

The following equation can be used to get the estimated data rate for a certain number of aggregated carriers, in a band or band combination, in 5G NR:

$$\text{Data Rate (Mbps)} = 10^{-6} \cdot \sum_{j=1}^{J} \left(\nu_{layers}^{(j)} \cdot Q_m^{(j)} \cdot f^j \cdot R_{\max} \cdot \frac{N_{PRB}^{BW(j),\mu} \cdot 12}{T_s^{\mu}} \cdot \left(1 - OH^{(j)}\right) \right), \quad (2.4)$$

where J is the amount of component carriers that make up a band or band combination, $\nu_{layers}^{(j)}$ represents the most supported layers possible, $Q_m^{(j)}$ indicates the highest supported modulation order. The scaling factor, or f^j, might have a value as low as 0.75 or as high as 1. R is the code rate and R_{max} = 948/1024. The number of PRBs is $N_{PRB}^{BW(j)}$, the sub carrier spacing (SCS) (as defined in TS 38.211) is represented by the NR numerology, which is μ. The average length of an orthogonal frequency division multiplexing (OFDM) symbol in a subframe for numerology is T_s^{μ}, and the $OH^{(j)}$ is the overhead set up by the upper layers, with the following values of 0.14 for FR1 DL, 0.08 for FR1 UL, 0.18 for FR2 DL and 0.10 for FR2 UL.

The number of information allocated resources, N_{RE}, and information, N_{info}, can be calculated as follows:

$$N_{RE} = N_{RE}^{'} \cdot N_{symb}^{sh} - N_{DMRS}^{PRB} - N_{oh}^{PRB}, \quad (2.5)$$

where $N_{RE}^{'}$ is given by:

$$N_{RE}^{'} = N_{SC}^{RB} \cdot n_{PRB}. \quad (2.6)$$

$$N_{info} = N_{RE} \cdot R \cdot Q_m \cdot \nu. \quad (2.7)$$

If $N_{info} \leq 3824$, one must determine $N_{info}^{'}$ through the following equation, and then verify table 2.2 to choose the appropriate transport block size (TBS) value, as follows:

$$N_{info}^{'} = max\left(24, 2^n \cdot \left[\frac{N_{info}}{2^n}\right]\right), \quad (2.8)$$

where the variable n is given by:

$$n = max\left(3, [log_2\left(N_{info}\right)] - 6\right). \quad (2.9)$$

For the cases when the condition $N_{info} \leq 3824$ is not satisfied, the values of n and $N_{info}^{'}$ are computed using the following set of equations:

$$n = \log_2\left(N_{info} - 24\right) - 5, \quad (2.10)$$

Table 2.2: TBS for 5G for $N_{info} \leq 3824$, adapted from [75]

Index	TBS	Index	TBS	Index	TBS	Index	TBS
1	24	31	336	61	1288	91	3624
2	32	32	352	62	1320	92	3752
3	40	33	368	63	1352	93	3824
4	48	34	384	64	1416		
5	56	35	408	65	1480		
6	64	36	432	66	1544		
7	72	37	456	67	1608		
8	80	38	480	68	1672		
9	88	39	504	69	1736		
10	96	40	528	70	1800		
11	104	41	552	71	1864		
12	112	42	576	72	1928		
13	120	43	608	73	2024		
14	128	44	640	74	2088		
15	136	45	672	75	2152		
16	144	46	704	76	2216		
17	152	47	736	77	2280		
18	160	48	768	78	2408		
19	168	49	808	79	2472		
20	176	50	848	80	2536		
21	184	51	888	81	2600		
22	192	52	928	82	2664		
23	208	53	984	83	2728		
24	224	54	1032	84	2792		
25	240	55	1064	85	2856		
26	256	56	1128	86	2976		
27	272	57	1160	87	3104		
28	288	58	1192	88	3240		
29	304	59	1224	89	3368		
30	320	60	1256	90	3496		

$$N_{info}^{'} = 2_n \cdot round\left(\frac{N_{info} - 24}{2_n}\right). \quad (2.11)$$

If the value of R is less than or equal to $\frac{1}{4}$, the TBS value is given by:

$$TBS = 8 \cdot C \cdot \left(\frac{N_{info}^{'} + 24}{8 \cdot C}\right), \quad (2.12)$$

where C is defined by:

$$C = \frac{N_{info}^{'} + 24}{3816}. \quad (2.13)$$

For the cases when $R \geq \frac{1}{4}$, if $N_{info}^{'} \geq 8424$ the value of C must be calculated using the following equation:

$$C = \frac{N_{info}^{'} + 24}{8424}. \quad (2.14)$$

For the same value of R, if $N_{info}^{'} \geq 8424$, the value of the TBS must then be determined by:

$$TBS = 8 \cdot \left(\frac{N_{info}^{'} + 24}{8}\right). \quad (2.15)$$

Chapter 3

Simulator Characterization and Performance Evaluation

3.1 5G-Air-Simulator

According to the authors from [76], the 5G-air-simulator is an open source and event-driven tool that simulates the essential components of the 5G air interface from a system-level viewpoint. The 5G-air-simulator is written in the C++ language, exploiting event-driven and object-oriented paradigms. It consists of more than 300 source and header files, 140 classes, and 60,000 lines of code. The source code is available at [77].
The main features of the well-known LTE-Sim tool [78], beginning with the object-oriented and event-driven paradigms, are carried over into the 5G-air-simulator. Additionally, it gains the ability to simulate various network environments at the system level as well as advanced and standard-compliant radio resource management techniques for both the control and user plane. Furthermore, by including new features and technological advancements that are better suited for 5G, the developed simulation framework significantly increases the previous project [76].
Figure 3.1 shows the important components of the proposed tool. According to [79], the fundamental building block of a simulator is its core, which offers all the steps required to perform object-oriented and event-driven paradigms as well as manage nodes, protocol stacks, mobility, and applications. The 5G-air-simulator includes a number of additional supporting models in addition to the simulator's main components, greatly expanding the functionality that LTE-Sim originally provided. Among these are the HARQ protocol, MIMO characteristics, and the calibrated and standard-compliant Link-To-System (L2S) model. These latter models provide an appropriate basis for the development of 5G technical components such as Massive MIMO, extended multicast/broadcast transmissions, predictor antennas, enhanced random access techniques, and NB-IoT.
Nine extended PLMs and seven baseline PLMs were included in the simulator first release. None of these, however, fits within the UMi_x scenarios listed in ITU-R Report M.2412-0 [10]. In this work, it is considered an updated version of the 5G-air-simulator, developed in our research group, which implements the UMi_A in LoS scenario, as presented in section 2.8, and is freely available under the GPLv3 license [80].

3.2 Capacity and Quality of Service

Mobile users (terminals) move throughout the service area and sometimes need communication services such as a wireless connection or packet transfer to and from a fixed network. This is known as a mobile access network, which is a wireless communication system. From

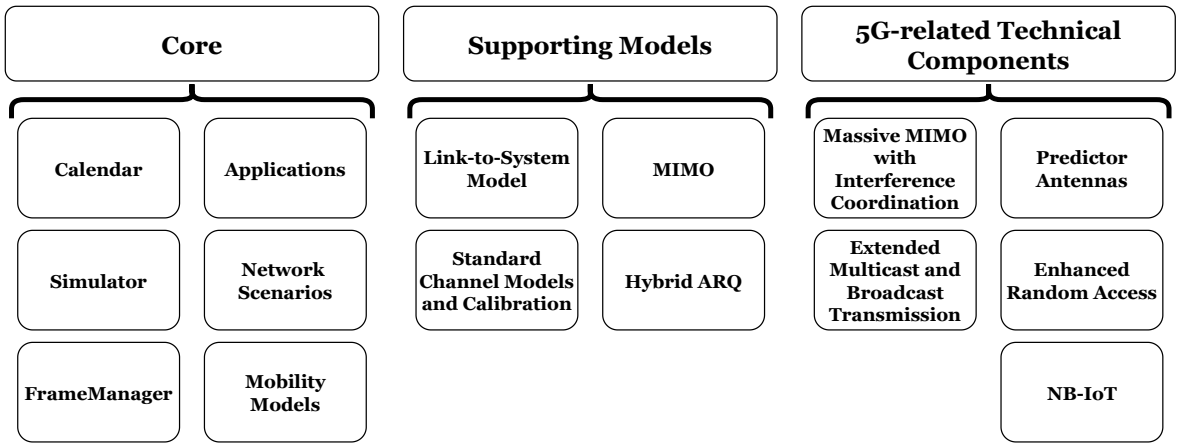

Figure 3.1: Building blocks of the 5G-air-simulator. Adapted from [79].

the perspectives of the user and the supplier, this has two separate aspects. The communication resources are owned by and made available to users by the network provider, or operator. The interests of the two entities are distinct. The user is determined to pay for the high-quality services they desire, while the operator wants to operate a successful company. The operator earnings will be maximized if they can increase the number of customers utilizing the system in the most basic scenario, where all users get the same service offering for the same price [81]. It also relies on economic aspects, like the cost and competitive operators or services offers, as well as the system technological limitations.

The term ”network capacity” is often used in an ambiguous manner to refer to a network ability to manage many users, and large amounts of data transmission. More specific definitions of the capacity are available depending on the type of the service offered. The greatest number of customers that the system can serve, in a basic scenario, with a single service and constant data rate, such as mobile telephony, may be referred to as the capacity. In a mobile data environment, the maximum total data rate that the system is capable of transferring might also be used to define capacity. The finest QoS, whether it is high speed data, small latency, or good voice quality, is what the user is looking for. It is worthwhile to note that services needing more resources per user will restrict the system capacity. These QoS requirements will, in general, affect capacity. Since the operator is the one who is paying for the system, it only makes sense that his viewpoint would determine the design process. The challenge will be to create systems where the profit, or cost/revenue, is maximized for particular service requirements of the user [81].

3.2.1 Scheduling

These days, wireless systems need to be built to meet a lot of brand-new specifications. For instance, wireless networks need to be able to provide high data rates, so that terminals may quickly access broadband services. Since terminals have been varying service needs, wireless networks should also have a flexible service architecture to combine several kinds services on a single air interface. Other sorts of services will get poor service quality if the network is exclusively optimized for one type of service. Effective QoS management strategies are

also required in addition to the flexible service design. For instance, there is a tight delay requirement for all video telephony, although the exact specifications might vary. When using multiple video resolutions, different rate and latency requirements must be met for delivering each packet [81].

If there were endless wireless resources, such as infinite spectrum, infinite transmission power, and infinite antennas, such that each terminal may be given the resources it demands, the needs of all terminals could be easily addressed. This is practically impossible due to a number of restrictions. As a result, wireless resources must be properly distributed across all terminals, and it is ideal to schedule their use in a way that maximizes the performance of the whole network [81].

In addition to the innovative capabilities and leading technology that 5G and beyond systems provide, efficient RRM is still essential for overcoming these limitations. More intelligent scheduling and resource allocation strategies, adaptable energy-saving methods, and smart mobility management will all be made possible by this RRM adaptability [82]. The QoS objectives are met, and the quality of the experience (QoE) for diverse consumers is improved by using an appropriate allocation of radio assets method [83].

In order to achieve an improved QoS, the RRM methods manage, operate, and share radio resources [83]. The frequency (bandwidth and carrier frequency), time (transmission duration), transmission power, and other system factors including antenna configuration and modulation/coding techniques, are used to describe radio resources [84]. In order to achieve the network's performance requirements, it effectively distributes the restricted frequency spectrum resources among the connected devices in a radio network area [83]. Before allocating the radio resources, the scheduling process takes the key performance indicator (KPI) restrictions specified for the scenario taken into account [85].

Schedulling strategies can be defined into two classes: content-aware and content-unaware strategies. The **content-aware** strategy refers to scheduling algorithms that take the content of the video streams into account and optimize the video using various techniques. Contrarily, **content-unaware** strategies refer to scheduling algorithms that take into consideration QoS factors (such as target delay, target throughput, and packet error rate) [86]. For content-unaware techniques, the radio resource management and packet scheduling options mostly are divided into two subclasses:

- **QoS-aware** - This method takes into consideration some network performance metrics in order to effectively employ the wireless systems resources, accurately schedule packets, and provide robust network performance parameters that would represent excellent QoS delivery to end users [86].

- **QoS-unaware** - This technique includes methods for allocating radio resources and scheduling packets for various users in wireless networks that take into account the fairness-controlling parameters, including the channel state information (CSI) and average data rate [86].

3.3 Radio and Simulation Parameters

A test scenario with a high user density and traffic loads that are concentrated on pedestrian users is taken into consideration to evaluate the system performance in a dense urban scenario. The dense urban environment is made up of a layer of microcells that are arranged in a regular hexagonal grid. The scenario considered in the 5G-air-simulator is a wrap-around of the 19 cell configuration, as shown in figure 3.2.

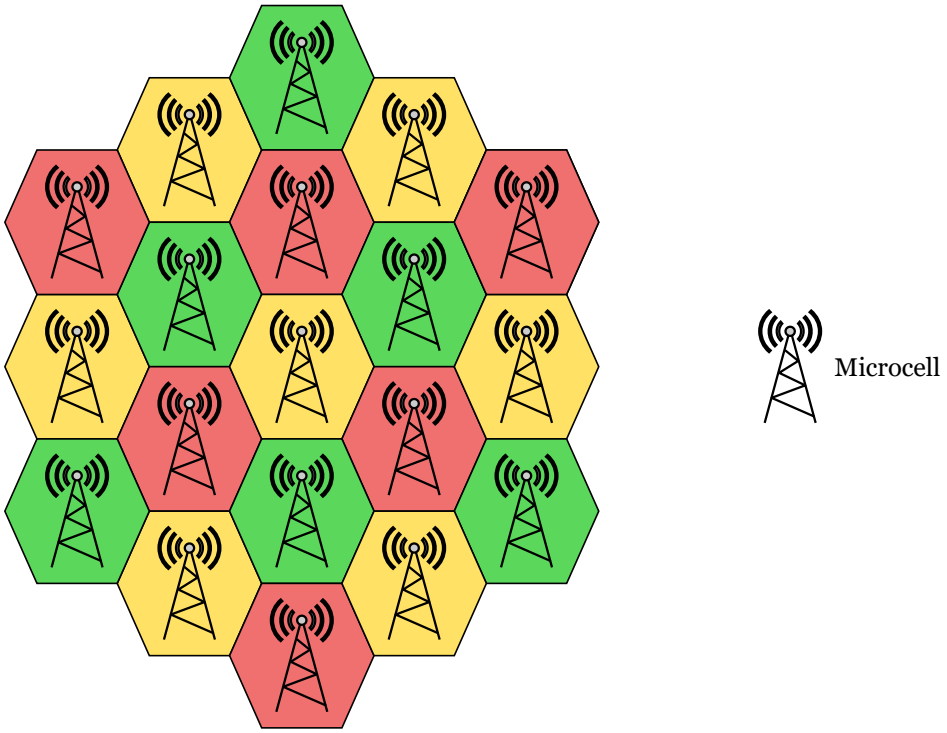

Figure 3.2: Nineteen microcells in hexagonal layout, where the own central cell and the interferer cells are represented in yellow.

The central cell in the simulations is the cell of interest, and users have only been deployed in there. In this work, the process for user deployment in the 5G-air simulator was updated, according to assumptions from [87], while assuming that users become uniformly distributed. The deployed users are not permitted to enter any nearby cells from the central cell. This work considers the reuse pattern three (k = 3). As illustrated in figure 3.3, only the cells highlighted in yellow which are utilizing the same set of sub-channels, impose interference onto the users at the central cell.

The node that offers coverage to users in the cell of interest is the gNB, shown in black. gNBs in red act as interferes. The ISD is the distance between a gNB and the nearest gNB, using the same set of sub-channels. In figure 3.2, each color presents a different set of sub-channels, and the $ISD = \sqrt{3k}R$, where R is the cell radius [88]. The availability of 20 MHz of spectrum per tier was considered.

In this work, the coverage and frequency reuse trade-off of the 5G NR operating bands (n7, n78, and n46) is analyzed. The radio and simulation parameters are presented in the table 3.1. These operating bands are in the FR1, which corresponds to frequencies from 410 MHz up to 7125 MHz, according to [89]. The center frequency for band n7 has been set at 2.6

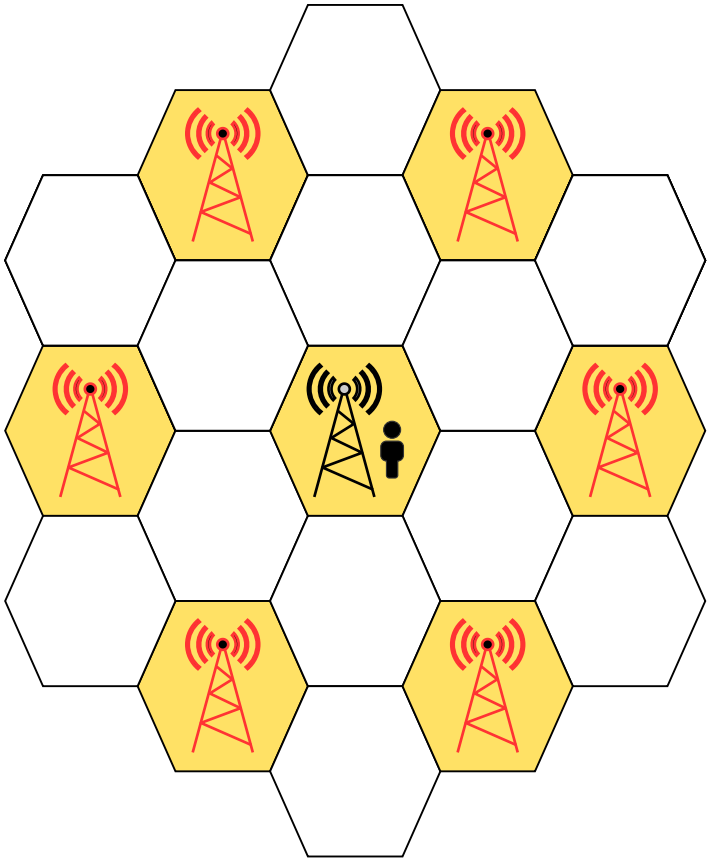

Figure 3.3: Cell of interest and interferer cells. Users are uniformly deployed in the central cell.

GHz, while the center frequencies for bands n78 and n46 are set at 3.5 GHz and 5.62 GHz, respectively.

In the recently deployed 5G networks, the 3.5 GHz frequency band has been chosen for the operator alongside mmW, mainly the 28 GHz band, which gives an understanding of the possibilities for spectrum sharing within this new technology while comparing the outcomes with LTE-based networks. It is possible to carry out experimental research using the 5.62 GHz frequency band as part of LTE-Unlicensed, which provides the opportunity of comparing the outcomes with those achieved by using licensed frequency bands, such as the 2.6 GHz band [31].

The obtained breakpoint distances for the 2.6 GHz, 3.5 GHz, and 5.62 GHz frequency bands, respectively, are 0.156 km, 0.21 km, and 0.3372 km when equation 2.3 is taken into account.

The considered numerology is 0. Numerology 0 corresponds to a subcarrier spacing of 15 kHz, according to [90]. Ten sub-frames make up this 15 kHz. Each sub-frame lasts 1 ms and each frame lasts 10 ms. There is one slot per sub-frame, and each slot carries 14 symbols.

The effective BS height (h_{BS}) in [10] might range from 1.5 m to 22.5 m. In the simulated deployment scenario, h_{BS} = 10 m has been taken into account. The effective UT height (h_{UT}) is 1.5 m. R ranges from 0.015 to 1 km. It is taken into consideration two packet scheduling techniques: a QoS-aware strategy performed by the M-LWDF scheduler and a QoS-unaware strategy performed by the PF scheduler [91]. One of the schedulers used the most by equipment suppliers is the PF. It is considered that UTs are always in LoS.

Table 3.1: Radio and Simulation Parameters

	Frequency Bands		
	2.6 GHz	3.5 GHz	5.62 GHz
NR operating band	n7	n78	n46
Numerology μ	0		
Subcarrier spacing [kHz]	15		
Number of subframes per radio frame	10		
Frame duration [ms]	10		
Number of slots per subframe	1		
Number of slots	10		
Number of symbols per slot	14		
Transmitter power small cells [dBm]	40.00	42.25	46.70
Transmitter power UT [dBm]	23		
Number of BS	19		
Reutilization	3		
Bandwidth per tier [MHz]	20		
Effective BS height [m]	10		
Effective UT height [m]	1.5		
Cell radius [km]	[0.015, 1]		
Scheduler	M-LWDF, PF		
Applications	VID and/or BE		
VID bit rate [Mb/s]	3.1		
Simulation duration [s]	46		
Flow duration [s]	40		
Number of simulations	50		

In one set of simulations, users are assumed to be downloading or viewing a VID stream with a 3.1 Mb/s bit rate. Each of the VID streams lasts 40 seconds, while the simulation lasts 46 seconds. Another set of simulations considered multi-service traffic with simultaneous use of VID+BE traffic. The number of simulations is 50 per number of users - value for the cell radius pair.

3.4 Results At The Saturation Level

The PLR represents the proportion of packets that are transferred compared to those that are lost in transport. In order to calculate results at saturation level (PLR<2%), the 3GPP TS 22.105 [32] for VID is used. In this TS, a critical performance target value for VID is established for a PLR with less than 2%. The suggested maximum end-to-end packet delay for VID is 150 ms, according to [32]. When determining the average values for delay, goodput, and FI, a target PLR<2% is taken into account.
The number of valuable information bits transmitted in a certain amount of time is known as the goodput [79]. Goodput does not include retransmitted data packets or overhead protocol bits, in contrast to throughput. The Jain's fairness index (FI) is taken into account in order to compare fairness. Fairness is defined as how shared resources are divided among users [92]. Lower fairness suggests that certain users are given preference over others, which could lead to a rise in the system's effectiveness. All users should have access to the necessary resources if fairness is high. The efficiency of the system may suffer degradation as a consequence of this fair access.
It is possible to achieve the most fair throughput distribution and the highest network throughput when all traffic flows have the same channel characteristics. In reality, the traffic flow channel conditions are often out of balance. As a result, the highest achievable throughput does not always follow from a maximally fair throughput distribution, and vice versa. In these circumstances, one may look for the best way to balance these two goals [93].
A well-known indicator for analyzing the fairness of resource distribution across traffic flows is the Jain's FI . It can be defined as:

$$FI = \frac{\left(\sum_{c \in C} R_c\right)^2}{|C| \sum_{c \in C} \left(R_c\right)^2}, \quad (3.1)$$

where C is the set of all data flows, i.e., $C = 1, 2, \ldots, |C|$. The values of FI lie in the range (0, 1] where a unity value indicates maximal fairness.
Three factors are taken into account during simulations: the number of users, R, and the scheduler. 50 simulations have been conducted to obtain statistical significance for each combination. It was used the strategy of beginning simulations with one user and raise this value in order to establish the saturation level. A further user was added, and 50 further simulation runs were done if the average PLR did not rise beyond 2%. User additions continued until the average PLR exceeded 2%. Each result is shown as an average with a 95% confidence interval. The confidence intervals are not shown in certain figures for readability reasons, since they are less than 1%.

3.4.1 Saturation Level For Video

3.4.1.1 Average Packet Loss Ratio

Results for the average PLR are shown in figures 3.4 and 3.5 for the M-LWDF and PF schedulers, respectively. The volatility in the number of users is a parameter in the PLR function that is expressed as a function of R. The horizontal purple line shows that the PLR is equal to 2%.

The behavior of the average PLR before and after the breakpoint distance can be observed when examining figures 3.4 and 3.5. The breakpoint distance increases with increasing frequency band, as shown by equation 2.3, and shown in section 3.3.

For Rs shorter than d'_{BP}, the average PLR reaches the longest values, as shown in figures 3.4a, 3.4b, and 3.4c.

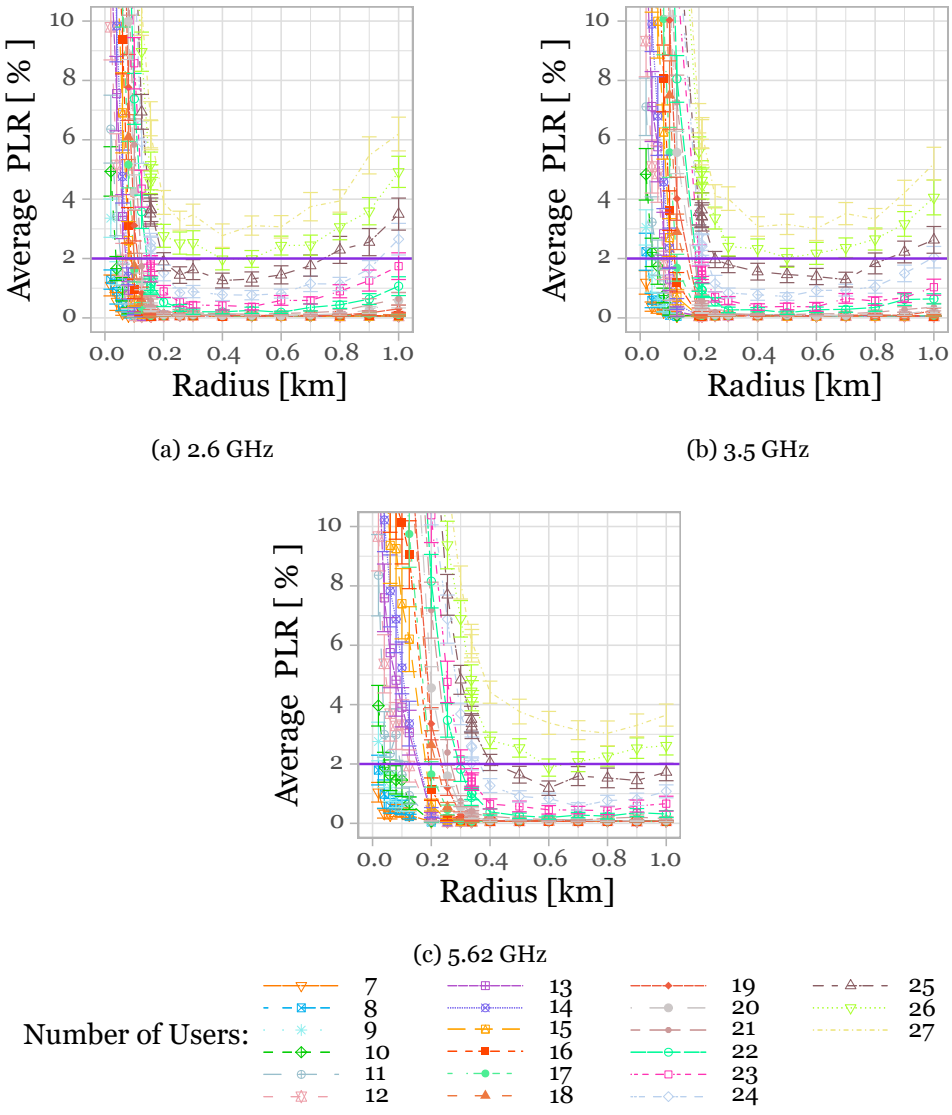

(a) 2.6 GHz

(b) 3.5 GHz

(c) 5.62 GHz

Figure 3.4: Results for the average PLR for the M-LWDF scheduler, as a function of R, with the number of users as a parameter (for different frequency bands). VID trace bit rate of 3.1 Mb/s.

When R increases, PLR goes down. The corresponding breakpoint distances are determined before the minimum values. The PLR improves for longer Rs after the minimum values are

achieved.

Results shown in figure 3.5 have been obtained by considering the PF scheduler. The PF scheduler exhibits the same behaviour as the the M-LWDF scheduler does. While the lowest values of PLR occur beyond the breakpoint distance, the higher values of PLR occur for shorter Rs. Beyond this value, the PLR rises for longer Rs. However, in general, the M-LWDF achieves lower values of the PLR for the same number of users.

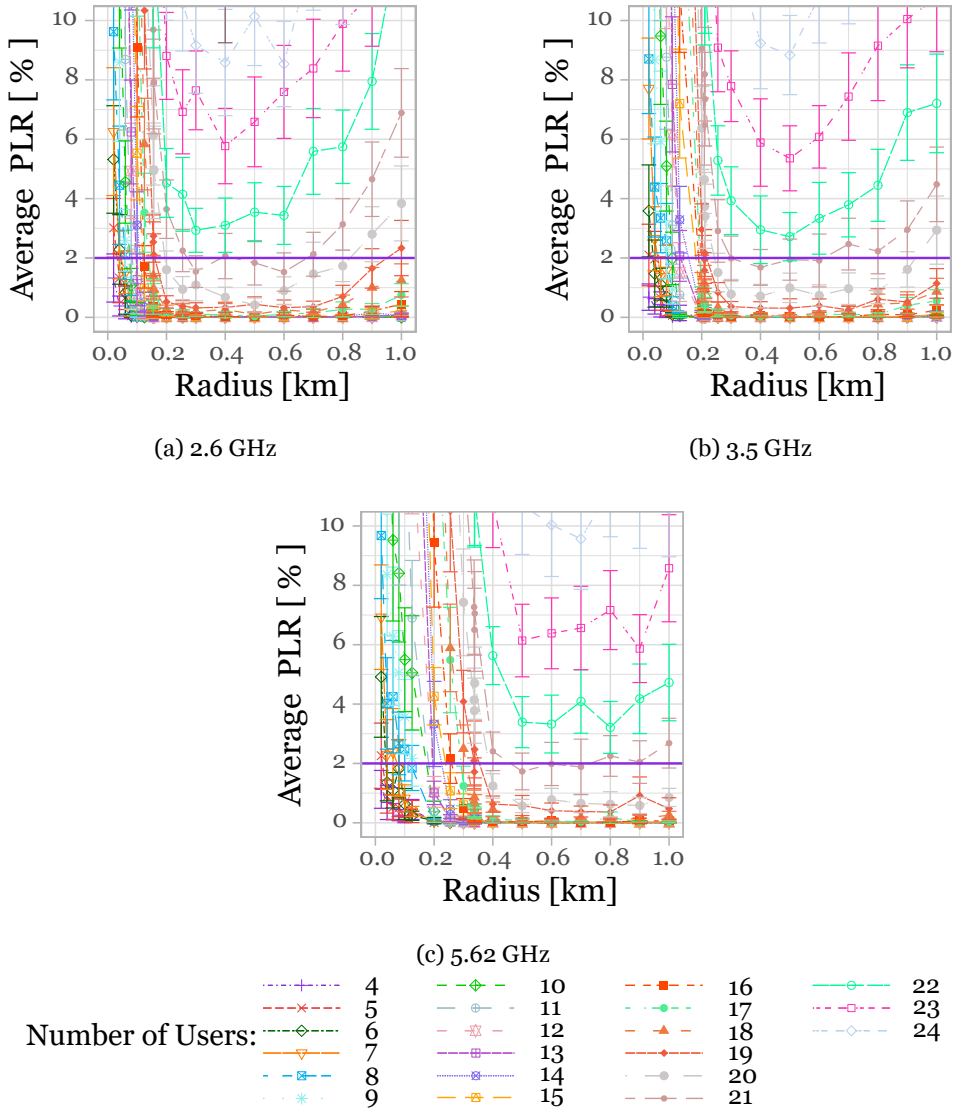

(a) 2.6 GHz

(b) 3.5 GHz

(c) 5.62 GHz

Figure 3.5: Results for the average PLR for the PF scheduler as a function of R, with the number of users as a parameter (for different frequency bands). VID trace bit rate of 3.1 Mb/s.

3.4.1.2 Maximum Average Delay

The maximum average delay is calculated only when the PLR is less than 2%. Figure 3.6 displays the outcomes for the M-LWDF scheduler as a function of R and the number of users as a parameter for various frequency bands. The largest values for the maximum delay are obtained when the values of R are near to the breakpoint distance. For longer Rs, the maximum delay also increases. Due to the increasing user density, there are initially more packet

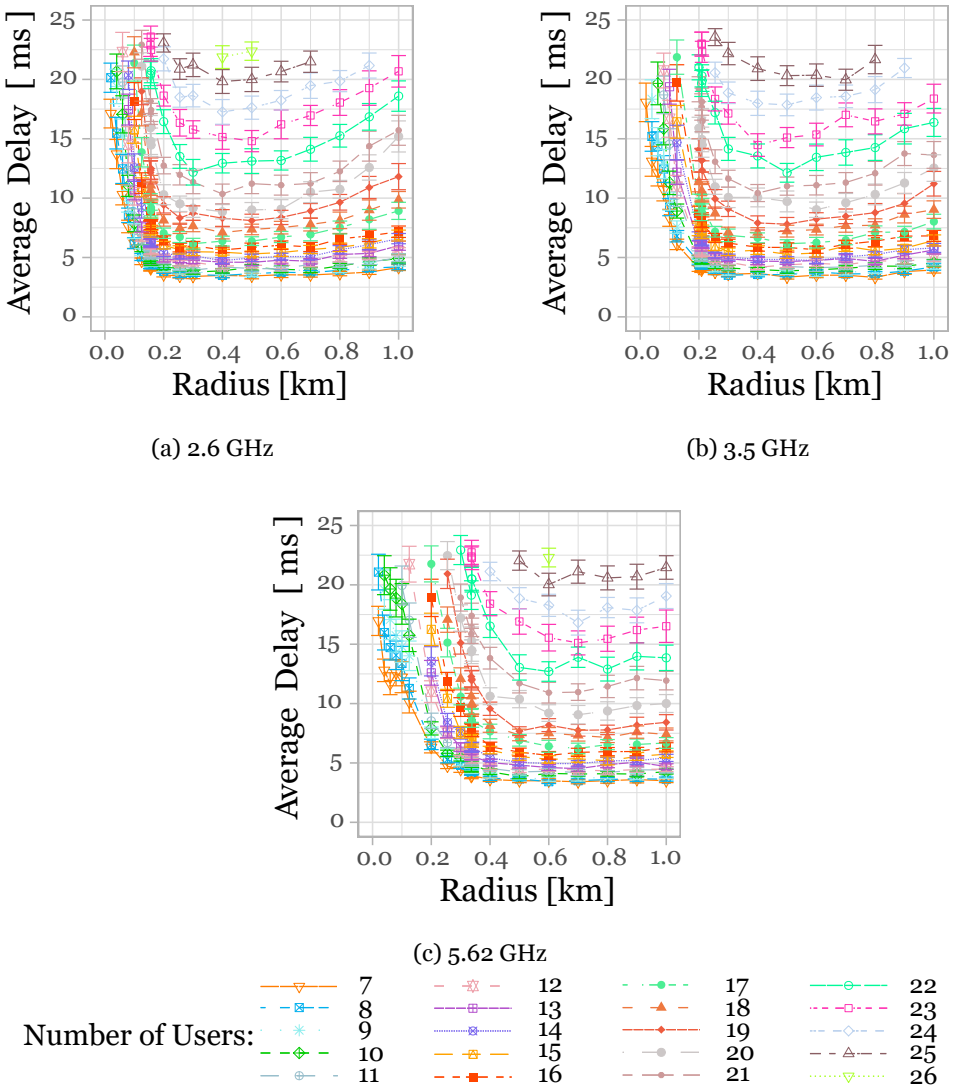

(a) 2.6 GHz

(b) 3.5 GHz

(c) 5.62 GHz

Figure 3.6: Results for the maximum average delay for the M-LWDF scheduler as a function of R with the number of users as a parameter (for different frequency bands). VID trace bit rate of 3.1 Mb/s.

collisions, which contribute to the delay. Beyond the breakpoint distance, due to the longest distances between the UT and the BS and resulting longer ISD (less interference), the average delay rises. For frequency bands of 2.6 GHz, 3.5 GHz, and 5.62 GHz, respectively, the longest average delay for the M-LWDF scheduler is between 22.5 ms and 25 ms for 23 UTs, 25 UTs, and 22 UTs, respectively.

Results for the maximum average delay considering the PF scheduler are presented in Fig. 3.7. The M-LWDF behaves similarly to the PF scheduler. The longest average delay values, how-

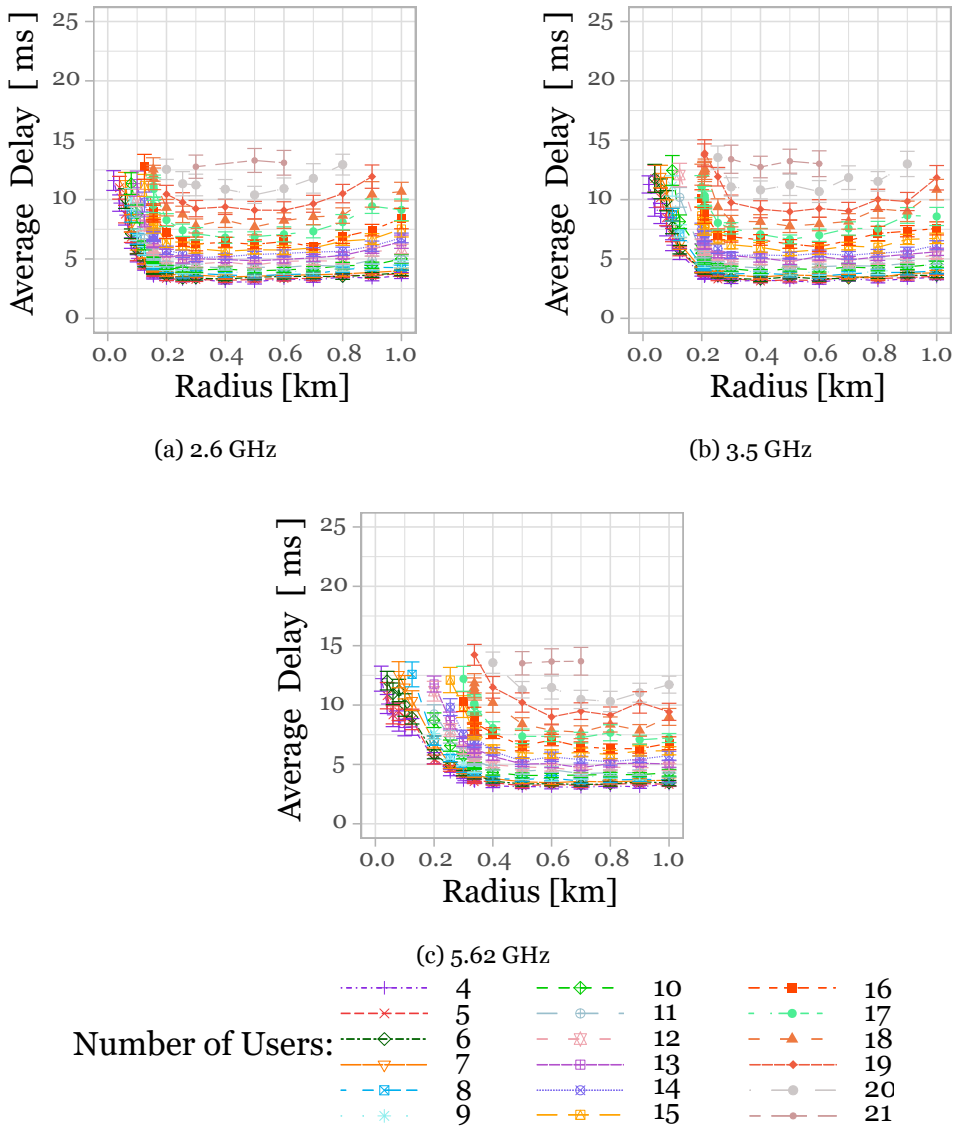

(a) 2.6 GHz

(b) 3.5 GHz

(c) 5.62 GHz

Figure 3.7: Results for the maximum average delay for the PF scheduler as a function of R with the number of users as a parameter (for different frequency bands). VID trace bit rate of 3.1 Mb/s.

ever, that can be achieved with the PF scheduler are between 12.5 ms and 15 ms for 21 UTs, 19 UTs, and 19 UTs, for the frequency bands of 2.6 GHz, 3.5 GHz, and 5,62 GHz, respectively. Which are circa 10 ms less than what was determined using the M-LWDF scheduler.

None of the schedulers reach the target maximum delay of 150 ms, for VID at the saturation level of PLR<2%. The maximum supported users may then be determined by extrapolating the highest values that correspond to a PLR of 2%. One can see from figure 3.4 that for

R=0.4 km and R=0.5 km, the 2.6 GHz frequency band is capable of supporting up to 26 users. From R=0.255 km up to R=0.8 km, 25 users may be supported at 3.5 GHz. In the highest frequency band (5.62 GHz), 26 users may be supported for $R \geq$0.6 km. However, compared to the M-LWDF scheduler, the PF scheduler supports considerably less users. For the simulated values of the cell radius of R=0.3 km, R=0.5 km and R=0.6 km, it is able to accommodate up to 21 users in the 2.6 GHz frequency band. 21 users may be supported at 3.5 GHz from a distance of R=0.3 km up to R=0.6 km. The higher frequency range of 5.62 GHz allows for the support of 21 users from a distance of R=0.5 km to R=0.7 km.

3.4.1.3 Maximum Average Fairness Index

As presented in section 3.4, the FI is used to to determine if users are receiving a fair share of system resources. A increase in system effectiveness may result from lower fairness, which implies that certain users are given priority over others. If fairness is high, all users should have access to the required resources. This fair access may have a negative impact on the system effectiveness. Results for the average FI take into account Jain's index. We have considered PLR<2%, as shown in figure 3.8. The resulting fairness index values for all Rs

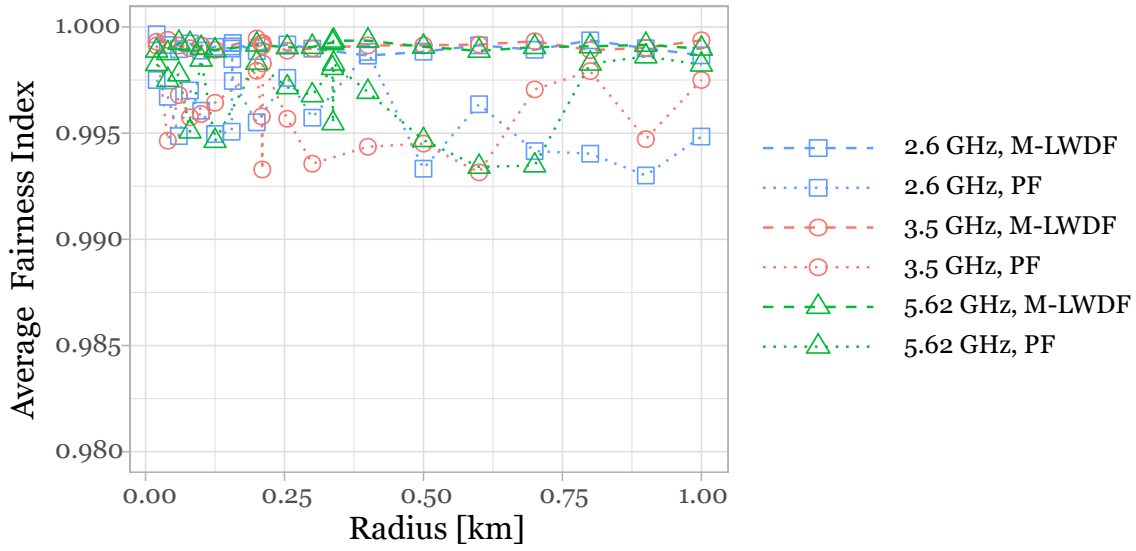

Figure 3.8: Maximum average fairness index for M-LWDF and PF schedulers, Only VID trace 3.1 Mb/s.

considered in the simulator are closer to 1, yet the M-LWDF is more reliable than the PF scheduler. For M-LWDF, the FI is close to 0.999. The typical values of the PF scheduler, which is unstable, are about 0.996. These results indicate that considering only results for PLR<2%, all supported users have access to the needed resources.

3.4.1.4 Maximum Average Cell Goodput

The goodput, as presented in section 3.4, is the number of useful information bits delivered per unit of time [79]. Differently from the throughput, goodput excludes overhead protocol bits and re-transmitted data packets. The average cell goodput when users are consuming VID flows may be calculated after finding the PLR and discarding all average values that did

not meet the requirement of PLR<2%, by choosing the number of users that corresponds to the highest average goodput, while checking whether the maximum average delay from figures 3.6 and 3.7 did not exceed the 150 ms limit. The derived results of the supported average throughput are presented in figure 3.9. With the M-LWDF scheduler, it is shown that

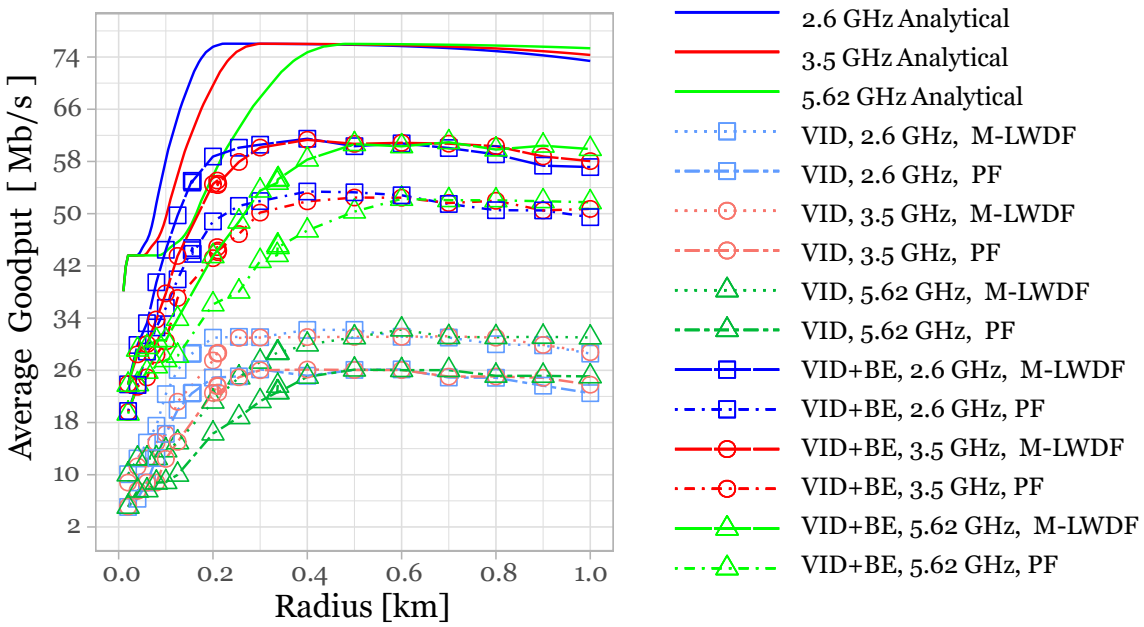

Figure 3.9: Maximum average goodput for M-LWDF and PF schedulers, Analytical, VID and VID+BE.

all frequency bands have a similar increasing behaviour from 0.02 km up to 0.04 km. The 2.6 GHz frequency band presents the highest values of the average cell goodput between 0.04 km and 0.5 km. Although the 2.6 GHz and 3.5 GHz seem to perform similarly at the Rs ranging between 0.255 km and 0.3 km, a numerical analysis shows an underlying modest advantage (when taking the 2.6 GHz band into account). The 5.62 GHz frequency band consistently displays highest values than the other two frequency bands for R>0.6 km.

Compared to the M-LWDF scheduler, the PF scheduler presents lower values for the average cell goodput. With the PF scheduler, the three frequency bands operate almost indistinguishably between 0.02 km and 0.06 km Rs. The 2.6 GHz frequency band offers the highest average cell goodput for radius up to 0.3 km. The 3.5 GHz frequency band surpasses the other two when R is equal to 0.4 km. For the longest Rs, the 5.62 GHz band presents the best average cell goodput.

The performance of the 2.6 GHz and PF scheduler is equal to the performance of the 5.62 GHz and M-LWDF scheduler when Rs is 0.08 m, according to a comparison of the two scheduler results. The average cell goodput values for the 3.5 GHz and PF scheduler begin to be greater than those for the 5.62 GHz and M-LWDF scheduler when R is 0.125 km. At 5.62 GHz, the M-LWDF scheduler only provides higher values for the average cell goodput when the R is longer than 0.255 km.

This leads us to the conclusion that, regardless of the scheduler being evaluated, the 2.6 GHz and 3.5 GHz frequency bands perform better than the 5.62 GHz for 0.08$\leq R\leq$0.255 km. This roughly occurs when the 2.6 GHz and 3.5 GHz frequency bands breakpoint distances are

exceeded. The M-LWDF scheduler produced the highest average cell goodput for the 5.62 GHz frequency band. For Rs beyond the breakpoint distance, with M-LWDF scheduler, the system capacity is increased by around 20%, with an average value of 32.25 Mb/s and R=0.6, compared to the PF scheduler.

Figure 3.10 shows the theoretical curves for the supported throughput as a function of the cell radius, for the 2.6, 3.5 and 5.62 GHz frequency bands, where R varies up to 1 km.

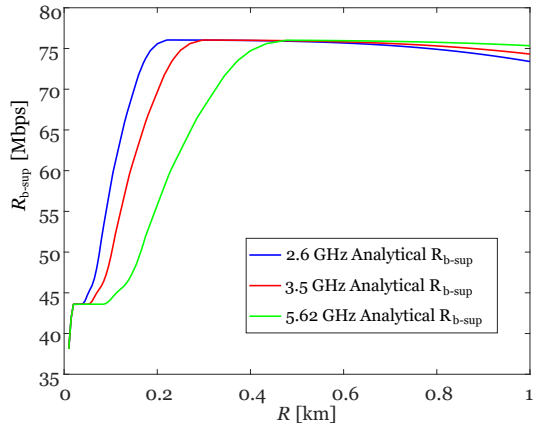

Figure 3.10: Equivalent supported throughput for the 2.6, 3.5 and 5.62 GHz frequency bands, for values of cell radius up to 1 km.

It is reasonable to conclude that there are underutilized resources from the combination of the comparable supported throughput results shown in figure 3.10 and the maximum average goodput for VID in figure 3.9.

The higher average cell goodput for VID is 32.25 Mb/s, while the comparable supported throughput is roughly 76 Mb/s. In the next subsection, simulations with VID+BE will be considered, so that a more reasonable comparison can be achieved as the average cell goodput will increase to values closer to the equivalent supported throughput.

When VID flows are taken into account, the maximum average delay, for the PF scheduler is shorter than the maximum average delay for the M-LWDF. In turn, the M-LWDF outperforms the PF scheduler in terms of highest average cell goodput and number of supported users. Addicitonaly, for longer Rs, for The 5.62 GHz frequency band performs better than the 2.6 GHz and 3.5 GHz bands for both schedulers. For shorter Rs, the 2.6 GHz frequency band performs better than the other two frequency bands. The M-LWDF is fairer than the PF, although somehow both schedulers perform similarly for the average FI.

3.4.2 Saturation Level with Video plus Best Effort

Given that for PLR<2% also BE flows are consumed, it is worthwhile to understand the use of the leftover resources that the VID application left behind. Authors from [78] claim that the BE application simulates a perfect source that always has packets to be sent, assuming that there are resources available.

3.4.2.1 Maximum Average Goodput

Results for this VID+BE combination are shown in figure 3.9 in terms of maximum average goodput. The maximum average goodput rises for both schedulers with the addition of BE. The M-LWDF goodput grows up to 61.4 Mb/s, whereas the PF goodput increases up to 53.3 Mb/s. When considering simply VID, the behavior is the same as when considering VID+BE. When using the M-LWDF scheduler instead of the PF scheduler, the system capacity is increased by around 20% for Rs longer than the breakpoint. With VID+BE and the PF scheduler, the system capacity is about 100% higher than with VID alone after the breakpoint distance. After the breakpoint, the system capacity with the M-LWDF scheduler is about 95% higher.

3.4.2.2 Maximum Average Fairness Index

Figure 3.11 displays the average FI for VID+BE results. The shortest Rs provided the largest

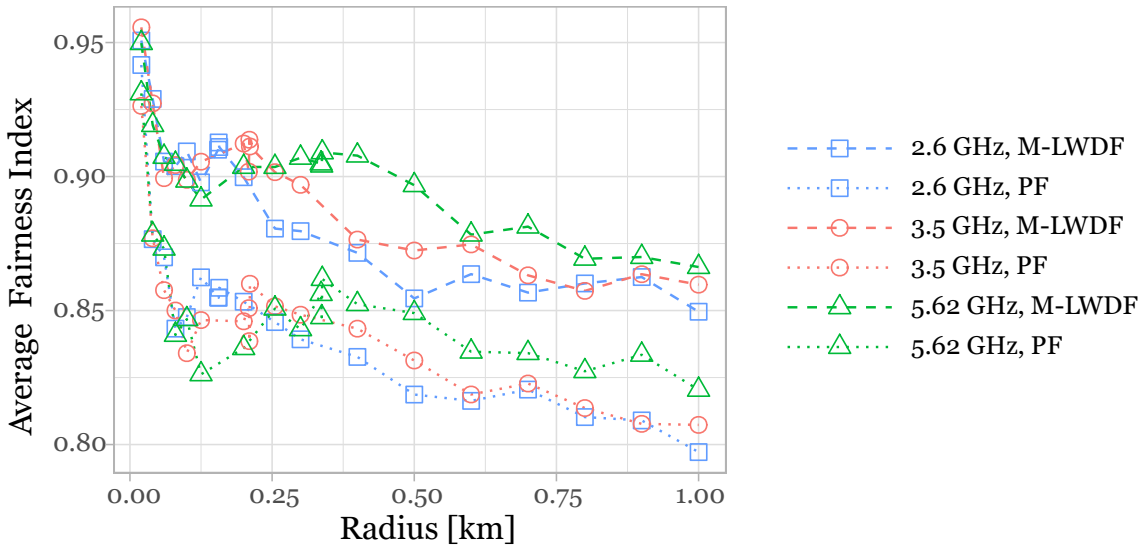

Figure 3.11: Average fairness index for M-LWDF and PF schedulers, VID+BE trace at 3.1 Mb/s.

values of the average FI. The average FI decreases as Rs become longer. When compared to when just VID was taken into account, the rise in average goodput means that more resources are being spent, and the overuse of resources causes the FI to fall. For the shortest Rs, due to the limited number of supported users, resources are divided more fairly as a consequence of the higher FI values. The frequency band with the largest FI values in both schedulers is 5.62 GHz (mainly for the longest Rs), followed by 3.5 GHz and then 2.6 GHz.

3.4.3 Lessons learned about the Saturation Level

As long as users are only consuming VID flows, resources are still available to be used by other types of services, up to the saturation level (i.e., values when PLR<2%). When VID+BE is taken into account, both schedulers use more available resources. Although, the PF scheduler still shows lower results in terms of average goodput, system performance may benefit

from adding the BE flows (more than for the M-LWDF scheduler). Performance-wise, the PF continues to go behind the M-LWDF.
On the other hand, the M-LWDF exhibits results that are more stable along the Rs than the PF, despite the fact that results for both schedulers are closer to one in terms of average FI. Due to the higher resource usage for VID+BE, the values achieved for the average FI are lower. The M-LWDF continues to perform better than the PF scheduler with VID+BE, even if the average FI also drops over the longest Rs.
Again, the 5.62 GHz frequency band outperforms the 2.6 GHz and 3.5 GHz for VID+BE with both scheduler, for the longest Rs. For shorter Rs, the performance of the 2.6 GHz frequency band is superior compared to the other two bands.

3.5 Results for the Maximum Cell Goodput with only BE

Although it was possible to achieve results for the maximum average goodput that were closer to the analytical supported throughput using the combination of VID+BE, there are still certain resources that need to be used. This occurs for both schedulers, although the M-LWDF clearly has an edge in terms of using the available resources.
The radio and simulation characteristics from table 3.1 have been taken into consideration in order to calculate the highest average goodput within the 5G-air-simulator can achieve for the UMi_A scenario. A total of 120 users have been considered for this simulation (evenly distributed over the center cell area). Only 10 BE flows are being consumed simultaneously by each user. This user and flow combination is the outcome of the initial trials carried out in the laboratory to reduce computing runtime. Other combinations could potentially result in the same kind of outcomes, but with a noticeable increase of the simulation time. Figure 3.12 presents the obtained results. Only PHY layer errors may cause packets to be lost since the BE only generates packets when the gNB schedules it to do so. As shown in figure 3.12a, the PLR trend for the BE flows is therefore very low. When R is 0.02 km, the maximum PLR is approximately 1.6%, and for longer Rs, the PLR decays to values of approximately 0.4%.
Both schedulers exhibit the same behavior in terms of the average goodput. The majority of the time, the average goodput difference is limited to tens of kbits. For the lowest Rs, the simulator presents lower goodput values than the analytical study, as shown in Fig. 3.12b, then the simulated goodput is higher than the analytical throughput. The highest average goodput that could be achieved was 72 Mb/s, while the highest analytical throughput was 76 Mb/s. The difference between the simulated goodput and the analytical throughput is explained since the simulator considers the mutual information effective signal to interference and noise ratio (SINR) mapping model (MIESM) and to obtain the analytical throughput is considered the SINR.
None of the schedulers exhibits superior performance to the other since the BE flows are not subject to any grade of service. When the R is equal to 0.7 km, the PF scheduler was able to achieve the highest average goodput of 72.197 Mb/s for the 3.5 GHz frequency band.
Figure 3.12c displays the results for the FI when the BE flows are taken into account to obtain the maximum cell goodput. The smaller Rs have provided the higher values for the FI. The FI

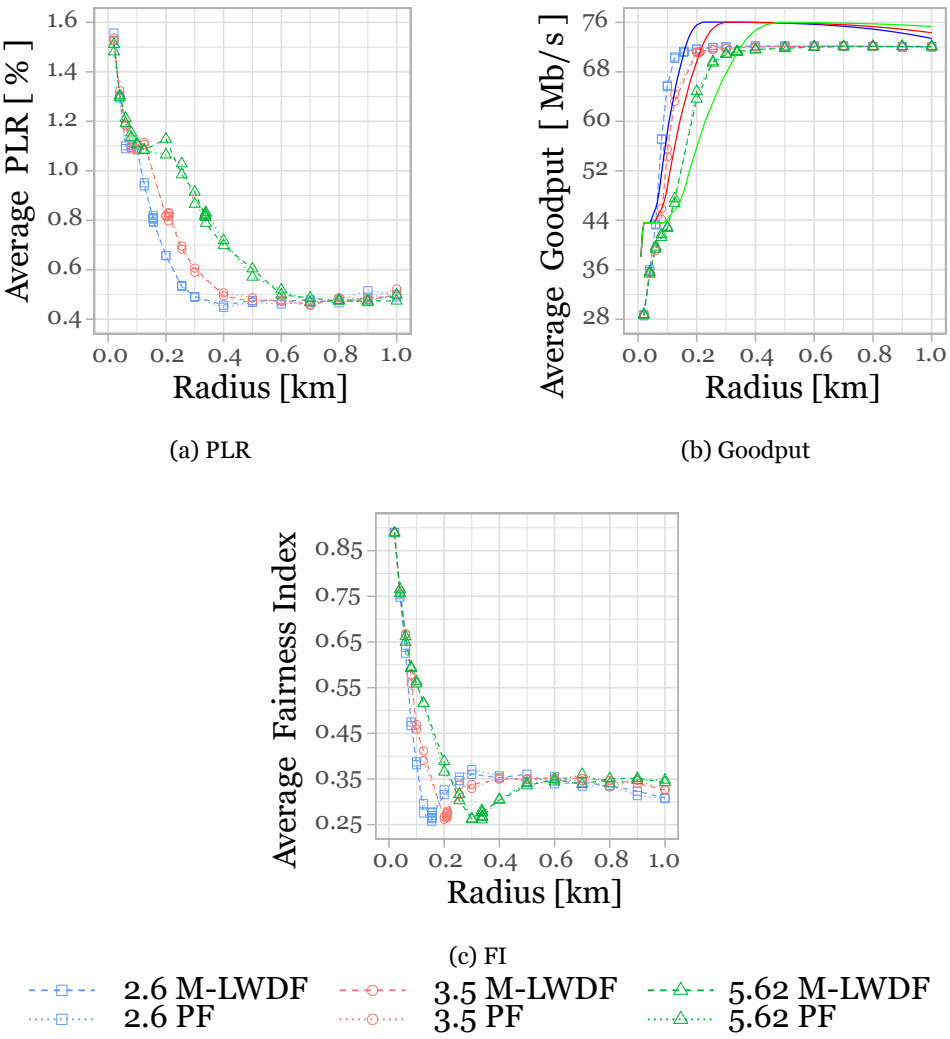

(a) PLR

(b) Goodput

(c) FI

Figure 3.12: Results for the maximum performance of the simulator. Only 10 BE flows are considered.

lowers as Rs becomes longer, either to the breakpoint distance or to Rs that is immediately closer. The FI grows beyond the breakpoint distance before decreasing once again. When comparing these results to those in figure 3.8, the fact that it was obtained lower fairness values indicates that the system is becoming more efficient. Since the BE is only scheduled if there are resources available, it is impossible to tell whether certain users are given preference over others while using BE flows.

3.6 Costs/Revenue Trade-off

From the perspective of many groups, including subscribers, network operators, service providers, regulators, and equipment suppliers, the economics of mobile radio networks may be examined as it is shown in figure 3.13 [94].

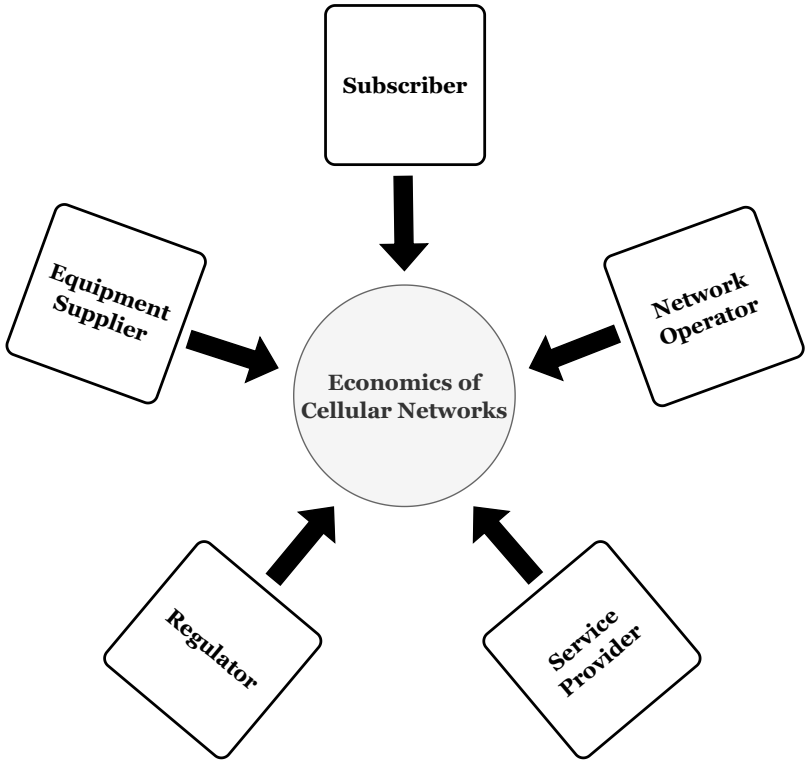

Figure 3.13: Four viewpoints of the economics of cellular networks. Adapted from [94].

The service quality and the cost associated with receiving the service are the main issues from the perspective of the subscriber. The subscriber is therefore more concerned with issues like the risk of calls being blocked, fixed costs (such as the price of the device, the activation fee, the monthly subscription fee), and variable costs related to the cost of the call and device maintenance (e.g. recharging or replacing the battery) [94]. The main goal of network operators and services providers is to increase his company profits. As a result, their objective is to determine the best configuration that would maximize his anticipated net profits [94]. Multimedia services available to user social welfare is a regulator's main concern. Therefore, the regulators goal is to guarantee both inexpensive public access to the services as well as effective and fair distribution of the restricted frequency spectrum to the

service providers [94]. Pricing the equipment is the main worry for a vendor (equipment suppliers) that supplies it to the service provider. The motivation for the service provider to buy the equipment from the vendor is minimal if the equipment's price is too high. In contrast, if the equipment is too cheaply priced, it can drive away customers from the vendor's sales of comparable products [94]. Availability of affordable prices of services (i.e., television and streaming) is the concern of the service providers.

The operator goals in the cellular planning process are to identify the best operating point that will maximize projected revenues. The technology to be employed, the size of the cell, and the number of channels to use in each cell are a few examples of the key aspects that need to be addressed [95].

The authors from [95], [96] and [97] propose to divide the cost of the system into two categories: capital costs (planning and setting up of a cell site) and operational costs (operation, management, and maintenance). On the one hand, capital costs include both fixed costs (such as licensing, fees, and spectrum auctions) and costs based on the quantity of BSs and transceivers, both of which are costs per unit of area. On the other hand, the operational expenses of the system, are partially determined by the quantity of transceivers and BSs per unit of area.

The system cost, C, per unit of area, €/km^2, is calculated as follows:

$$C = C_{fi} + C_b \cdot N, \quad (3.2)$$

where C_{fi} is the fixed terms of the costs, C_b is the cost per gNB and N is the number of hexagonal coverage zones per unit of area, 1/km^2, defined by the following equation:

$$N = \frac{2}{3 \cdot \sqrt{3} \cdot R^2}. \quad (3.3)$$

The C_{fi}, in €/km^2, is calculated as follows:

$$C_{fi} = \frac{\frac{LicPrice}{A_{Country}}}{N_{year}}, \quad (3.4)$$

where the $LicPrice$ represents the price of the license and spectrum auction fees, in €, $A_{Country}$ is the country area, in km^2, and N_{year} is the project lifetime, in years.

The cost per gNB, C_b, in €, is defined by:

$$C_b = \frac{C_{BS} + C_{bh} + C_{FHplusBBU} + C_{inst}}{N_{year}} + C_{M\&O}, \quad (3.5)$$

where the C_{BS} is the cost of the BS/RRH itself, in €, C_{bh} is the BH cost, in €, the C_{inst} is the cost of the installation, in €, and $C_{M\&O}$ is the cost of maintenance and operation, in €. $C_{FHplusBBU}$ is the cost of the FH plus the BBU (i.e., the total cost of the BBU in one-to-one configurations or part of the cost of the BBU in one-to-many configurations), and is

represented by the following equation:

$$C_{FHplusBBU} = C_{FH} + \frac{C_{RRHplusBBU}}{N_{RRH}}, \quad (3.6)$$

where C_{FH} is the cost of the FH, in €, $C_{RRHplusBBU}$ is the cost of the RRH plus the BBU, in €, and the N_{RRH} is the number of RRHs used. Which is one for one-to-one or and integer value higher than one for one-to-many configurations.
The revenue per unit of area, R_v, can be obtained by:

$$R_v = \frac{N \cdot R_{b-sup} \cdot T_{bh} \cdot R_{R_b}}{R_{b-ch}}, \quad (3.7)$$

where N is the number of hexagonal cells, R_{b-sup} is the supported goodput per BS, in kb/s, R_{R_b} is the revenue of a channel with data rate R_b, in €/min, R_{b-ch} is the bit rate of the channel, in kb/s, and T_{bh} is the equivalent duration of busy hours per day, calculated with the follow equation:

$$T_{bh} = 60 \cdot 6 \cdot 240, \quad (3.8)$$

where we considered 60 as an hour in minutes, 6 busy hours per day, and 240 busy days per year.
The difference between the revenue per unit of area and the system costs allow for obtain the profit, by dividing the profit by the system cost, one obtains the profit in percentage terms, $P_{[\%]}$:

$$P_{[\%]} = \frac{R_v - C}{C} \cdot 100. \quad (3.9)$$

For the optimization process it is important to consider the functional split options, the following ones are used: split option 7.2 (intra-PHY) and split option 6 (MAC-PHY). Split option 7.2, which lowers the amount of traffic between DU and RU, was selected by O-RAN, who defined a version of their own termed 7.2x split as the ideal combination between quickly getting this technology to market, and implementation cost [98]. On the other hand, split option 6 is beneficial for small cells [99].
The Tab. 3.2 lists the parameter values for the equations stated for estimating costs, revenues, profits, and other metrics. Fig. 3.14 shows the profit in percentage terms for the PF and M-LWDF scheduler, while considering VID and VID+BE traffics, as well as the applicability or not of the functional splits.
With VID, the outcome for the 2.6 GHz frequency band is as follows:

- On the one hand, for the M-LWDF scheduler, the highest achievable profit without splitting, is 73.61%. On the other hand, for the PF scheduler the profit in percentage terms is 41.12%. The lowest profits are -45.49% for the M-LWDF scheduler and -72.62% for the PF scheduler.

- On the one hand, with a split 6 applied, the maximum profit that can be obtained, for the M-LWDF scheduler is 143.98%. On the other hand, for the PF scheduler, the

Table 3.2: Radio and Simulation Parameters for UMi_A

Costs		Without Splitting	Split 6	Split 7.2
$LicPrice$ [€]	2.6 GHz	6 000 000		
	3.5 GHz	4 880 000		
	5.62 GHz	0		
$A_{Country}$ [km^2]		92 212		
N_{year}		5		
C_{BS} [€]		5 700 (100%)	1 425 (25%)	1 140 (20%)
C_{BH} [€]		2 000		
C_{FH} [€]		2 000		
C_{inst} [€]		400		
N_{RRH}		6		
$C_{RRHplusBBU}$ [€]		0	6 400	8 000
$C_{FHplusBBU}$ [€]		2 000	3 066	3 333.33
$C_{M\&O}$ [€]		200		
R_{R_b} [€/min]		0.000 2		
R_{b-ch} [kb/s]		144		

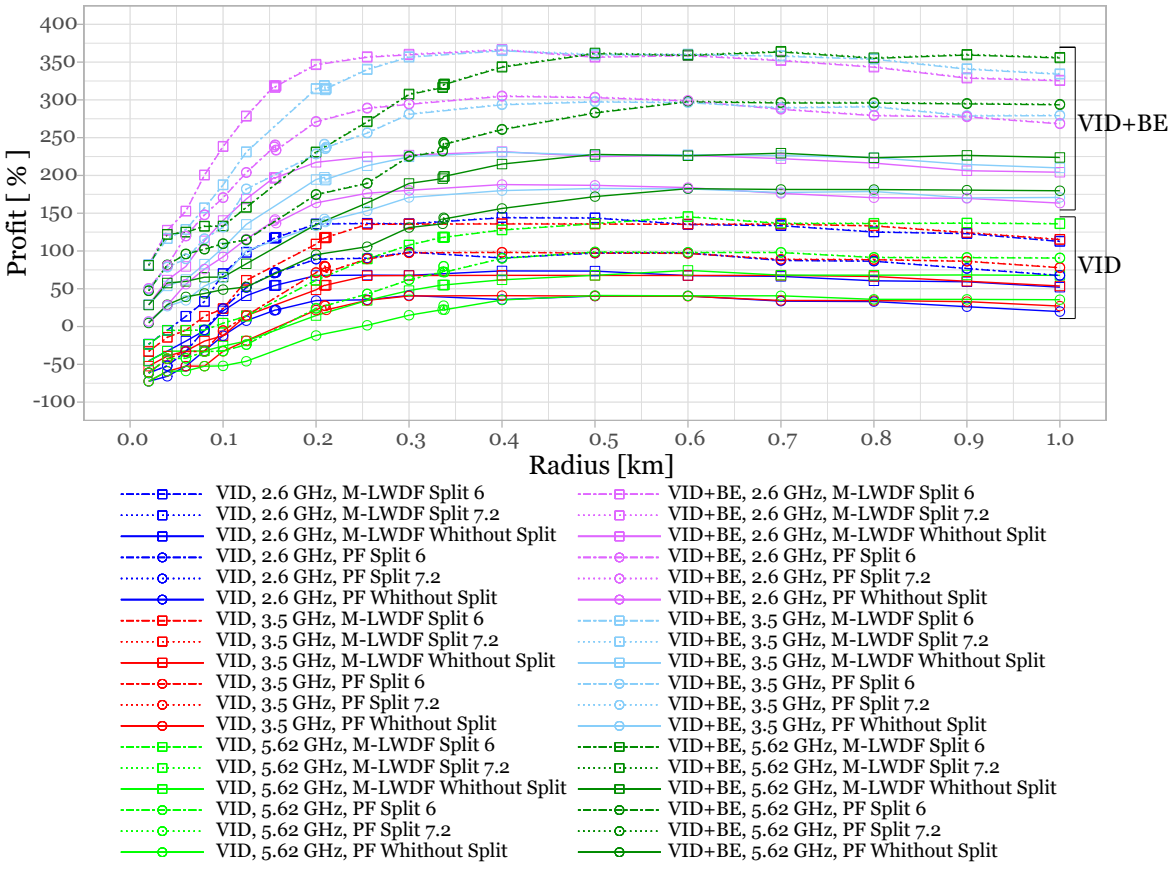

Figure 3.14: Profit for PF and M-LWDF schedulers in VID and VID+BE.

profit in percentage terms is 98.40%. The lowest profits are -23.32% for the M-LWDF scheduler and -61.48% for the PF scheduler.

- On the one hand, for the M-LWDF scheduler, the highest profit possible with a split 7.2 applied, is 144.52%. On the other hand, for the PF scheduler it is 98.84%. The minimum profits are -23.14% for the M-LWDF scheduler and -61.40% for the PF scheduler.

With VID+BE, the outcome for the 2.6 GHz frequency band is as follows:

- On the one hand, for the M-LWDF scheduler, the highest achievable profit, without splitting, is 231.52%. On the other hand, for the PF scheduler the profit in percentage terms is 187.91%. The lowest profits are 28.92% for the M-LWDF scheduler and 6.85% for the PF scheduler.

- On the one hand, with a split 6 applied, the maximum profit that can be obtained, for the M-LWDF scheduler is 365.88%. On the other hand, for the PF scheduler, the profit in percentage terms is 304.61%. The lowest profits are 81.35% for the M-LWDF scheduler and 50.31% for the PF scheduler.

- On the one hand, for the M-LWDF scheduler, the highest profit possible with a split 7.2 applied, is 366.92%. On the other hand, for the PF scheduler it is 305.51%. The minimum profits are 81.75% for the M-LWDF scheduler and 50.64% for the PF scheduler.

With VID, the outcome for the 3.5 GHz frequency band is as follows:

- On the one hand, for the M-LWDF scheduler, the highest achievable profit, without splitting, is 67.75%. On the other hand, for the PF scheduler the profit in percentage terms is 40.90%. The lowest profits are -52.40% for the M-LWDF scheduler and -72.31% for the PF scheduler.

- On the one hand, with a split 6 applied, the maximum profit that can be obtained, for the M-LWDF scheduler is 135.78%. On the other hand, for the PF scheduler, the profit in percentage terms is 98.04%. The lowest profits are -33.05% for the M-LWDF scheduler and -61.06% for the PF scheduler.

- On the one hand, for the M-LWDF scheduler, the highest profit possible with a split 7.2 applied, is 136.31%. On the other hand, for the PF scheduler it is 98.48%. The minimum profits are -32.90% for the M-LWDF scheduler and -60.97% for the PF scheduler.

With VID+BE, the outcome for the 3.5 GHz frequency band is as follows:

- On the one hand, for the M-LWDF scheduler, the highest achievable profit, without splitting, is 230.76%. On the other hand, for the PF scheduler the profit in percentage terms is 182.75%. The lowest profits are 29.29% for the M-LWDF scheduler and 5.97% for the PF scheduler.

- On the one hand, with a split 6 applied, the maximum profit that can be obtained, for the M-LWDF scheduler is 364.90%. On the other hand, for the PF scheduler the profit in percentage terms is 297.23%. The lowest profits are 81.87% for the M-LWDF scheduler and 49.06% for the PF scheduler.

- On the one hand, for the M-LWDF scheduler, the highest profit possible with a split 7.2 applied, is 365.94%. On the other hand, for the PF scheduler it is 298.12%. The minimum profits are 82.27% for the M-LWDF scheduler and 49.40% for the PF scheduler.

With VID, the outcome for the 5.62 GHz frequency band is as follows:

- On the one hand, for the M-LWDF scheduler, the highest achievable profit, without splitting, is 74.31%. On the other hand, for the PF scheduler the profit in percentage terms is 41.12%. The lowest profits are -45.71% for the M-LWDF scheduler and -72.52% for the PF scheduler.
- On the one hand, with a split 6 applied, the maximum profit that can be obtained, for the M-LWDF scheduler is 145.19%. On the other hand, for the PF scheduler the profit in percentage terms is 98.51%. The lowest profits are -23.63% for the M-LWDF scheduler and -61.36% for the PF scheduler.
- On the one hand, for the M-LWDF scheduler, the highest profit possible with a split 7.2 applied, is 145.74%. On the other hand, for the PF scheduler it is 98.95%. The minimum profits are -23.46% for the M-LWDF scheduler and -61.27% for the PF scheduler.

With VID+BE, the outcome for the 5.62 GHz frequency band is as follows:

- On the one hand, for the M-LWDF scheduler, the highest achievable profit, without splitting, is 229.44%. On the other hand, for the PF scheduler the profit in percentage terms is 182.50%. The lowest profits are 28.48% for the M-LWDF scheduler and 4.66% for the PF scheduler.
- On the one hand, with a split 6 applied, the maximum profit that can be obtained, for the M-LWDF scheduler, is 363.41%. On the other hand, for the PF scheduler the profit in percentage terms is 297.38%. The lowest profits are 80.73% for the M-LWDF scheduler and 47.21% for the PF scheduler.
- On the one hand, for the M-LWDF scheduler, the highest profit possible with a split 7.2 applied, is 364.45%. On the other hand, for the PF scheduler it is 298.27%. The minimum profits are 81.14% for the M-LWDF scheduler and 47.55% for the PF scheduler.

3.6.1 Lessons Learned

This contribution provides a set of analytic results for the cost/revenue trade-off while comparing deployments without functional splitting with scenarios for functional split 7.2 or 6 are applied. The use of VID or VID+BE traffic is assumed and the performance is compared between three frequency bands (2.6 GHz, 3.5 GHz and 5.62 GHz). The outcome of this cost/revenue trade-off analysis, shows that, with split 7.2 applied, the maximum profits are obtained at a radius of 0.4 km for the 2.6 GHz frequency. In the case of the M-LWDF scheduler, the profit is 366.92%. For the PF scheduler it is 305.51%. For the same cell radius and scheduler, the profit with split 7.2 applied is always slightly higher than the profit in percentage terms with a split option 6. The profit is growing up to the breakpoint. However, the

profit tends to be larger beyond the breakpoint distance. For the M-LWDF scheduler, for the same radius and functional split option, the profit is always higher than for the PF scheduler. In the case of VID+BE the profit is never negative or null although for the 0.02 km radius the minimum profit is 4.66% at 5.62 GHz, when the PF scheduler is applied without functional splitting. However in the case of VID traffic the profit only becomes positive at circa 0.06 km cell radius, with values of 13.78% and 13.53%, for the 2.6 GHz frequency and the M-LWDF scheduler with the splits 7.2 and 6, respectively.

Chapter 4

Conclusions and Topics for Further Research

4.1 Conclusions

This dissertation proposes to determine the service quality metrics (e.g., packet loss ratio, PLR, average delay, fairness index, FI) the highest data rate achievable when a numerology zero is considered, for three frequency bands (2.6 GHz, 3.5 GHz, and 5.62 GHz). 5G New Radio (NR) is considered for an urban micro (UMi) cell scenario where the frequency range is between 0.5 and 7 GHz, and the chosen propagation model is model A (UMi_A). In order to determine radio and network performance, the UMi_A model was implemented in the 5G-air-simulator. It is possible to determine the saturation level using the results for the PLR. According to the 3rd Generation Partnership Project (3GPP), saturation occurs when the PLR is lower than 2% for video (VID) services. The values for the delay, maximum number of supported users, FI and goodput were obtained considering PLR$<$2%, and all this values are presented in average terms. This work also studies the performance of two schedulers in terms of quality of service (QoS): The QoS-aware modified largest weighted delay first (M-LWDF) scheduler and the QoS-unaware proportional fair (PF) scheduler.
For the VID case, along the considered cell radius, Rs, from 0.015 km up to 1 km, for the same simulated number of users, the M-LWDF presents lower values for the PLR than the PF scheduler. We found the highest values for the PLR for the shortest Rs. With the increase in R, we found that the PLR decreases while minimums are simulated after the respective breakpoint distance, $d_{BP}^{'}$. We observed that, as the R increased, after the $d_{BP}^{'}$, so did the PLR. It was considered the PF and found that the first increase in PLR and then decrease and again increase with the change of (high value) R. This behavior of PLR is more visible for the 2.6 GHz frequency band, and for the 3.5 GHz. While for the 5.62 GHz it is almost not noticed. Taking into account the target PLR<2%, the PF obtained lower values for the delay. As for the M-LWDF scheduler, the maximum average delay is between 22.5 ms and 25 ms, while for the PF scheduler it is as low as 12.5 ms and 15 ms. The average delay never surpassed the maximum value of 150 ms appointed by 3GPP for video services. M-LWDF scheduler supports more users than the PF scheduler. For the M-LWDF scheduler, the 2.6 GHz frequency band is capable of supporting up to 26 user, the 3.5 GHz band supports 25 user, and the 5.62 GHz band supports 26 user. While the PF can support a maximum of 21 users. For both schedulers, the FI is closer to one. This means that all users had access to the needed resources. The M-LWDF scheduler presents higher values of the average goodput than the PF scheduler. Accounting for the maximum average cell goodput, we may conclude that the 2.6 GHz and 3.5 GHz frequency bands perform better than the 5.62 GHz, apart from scheduler selection (0.08 km Rs up to 0.255 km). With the M-LWDF scheduler, the maximum obtained average goodput was around 32.25 Mb/s for the 5.62 GHz frequency band,

and that is less than half of the analytical equivalent supported throughput which reaches 76 Mb/s, while for PF scheduler the maximum obtained average goodput is 25 Mb/s for 0.6 km R. As a result of FI, we see the M-LWDF provide stability over the PF. When VID traffic is considered done, we can conclude that there are resources that are not utilized.
To consume the remaining resources, a best effort (BE) flow was added to each user. With this procedure, with the M-LWDF scheduler, the average goodput increases up to 61.4 Mb/s and up to 53.3 Mb/s with the PF scheduler. The average FI presents a decay for longer values of R. One can conclude that, this combination of video plus best effort (VID+BE) brought the consumption of resources closer to the analytical equivalent supported throughput. To determine the maximum average cell goodput, with 5G-air-simulator, a combination of 120 uniformly distributed users, each one consuming 10 BE flows, was considered. With this combination of users and traffic usage, the average PLR never achieved the 2% target value. The maximum value was closer to 1.6% for the 0.02 km R. For Rs shorter than the $d_{BP}^{'}$, the simulator achieves lower values for the average cell goodput. In turn, for longer Rs, the analytical equivalent supported throughput is higher. The difference between the simulated average cell goodput and the analytical throughput is explained since the simulator considers the mutual information effective signal to interference and noise ratio (SINR) mapping (MIESM) model, but to obtain the analytical supported throughput, only the SINR is considered. Throughout all the work, the 2.6 GHz frequency band performs better for the shortest Rs, while the 5.62 GHz performs better for the longest Rs.
The costs, revenues, profit in percentage terms, and other metrics have been estimated as well for the PF and M-LWDF schedulers in VID and VID+BE, with or without consideration of the functional split options 7.2 and 6, for three frequency bands (2.6 GHz, 3.5 GHz and 5.62 GHz). By deploying the 19 cells, the simulation results are first established. These findings are used to analyze the goodput, the number of supported users, and PLR for three frequency bands. Then, with consideration of goodput, an amount of supported users, and PLR for 2.6 GHz, 3.5 GHz, and 5.62 GHz, a cost and trade-off analysis for splits 7.2 and 6 is examined. It was found that for the same radius and scheduler, the profit with a split 7.2 applied is always slightly higher than the profit in percentage terms with a split option 6. The profit is growing up to the breakpoint. However, the profit tends to be larger beyond the $d_{BP}^{'}$. For the M-LWDF scheduler, for the same radius and functional split option, the profit is always higher than for the PF scheduler. In the case of VID+BE the profit is never negative or null although for the 0.02 km radius the minimum profit is 4.66% at 5.62 GHz, when the PF scheduler is applied without functional splitting. However in the case of VID traffic the profit only becomes positive at circa 0.06 km cell radius, with values of 13.78% and 13.53%, for the 2.6 GHz frequency and the M-LWDF scheduler with the splits 7.2 and 6, respectively.

4.2 Proposals of further research

This work addresses 5G NR small cell networks for an UMi cell scenario, where the frequency range is between 0.5 and 7 GHz. Simulations have been performed with the 5G-air-simulator. The achievable system capacity has been explored when a numerology zero is considered.

Two packet schedulers have been compared in terms of QoS. In the study of the cost/revenue trade-off for the PF and M-LWDF schedulers, by considering VID and VID+BE traffic, with or without consideration of the functional splits (7.2 and 6), for the three considered sub-6 GHz frequency bands, some limitations have been identified.
As a future work, regarding this research, one possibility is to address the cost/revenue trade-off for the other functional split options while comparing them.
In centralized radio access network (C-RAN), we have remote radio heads (RRH) connected to the base band unit (BBU) pool, using the fronthaul links. Considering the scenario one to many (when the BBU is connected to multiple RRHs), the power consumption and complexity of the shared BBU can be reduced if the user is unavailable or the traffic is low, because the nearby cell zooms out while the quiet cells sleep. One possibility of future work is to take this energy consumption approach in small cells scenarios into account, and adapt it to the simulator. Topologies where each BBU (or centralized unit plus distributed unit) serves one (one to one) or several (one to many) RRHs can be considered.

References

[1] M. Kalil, A. Al-Dweik, M. F. Abu Sharkh, A. Shami, and A. Refaey, "A Framework for Joint Wireless Network Virtualization and Cloud Radio Access Networks for Next Generation Wireless Networks," *IEEE Access*, vol. 5, pp. 20 814–20 827, 2017. 1

[2] D. Wubben, P. Rost, J. S. Bartelt, M. Lalam, V. Savin, M. Gorgoglione, A. Dekorsy, and G. Fettweis, "Benefits and Impact of Cloud Computing on 5G Signal Processing: Flexible centralization through cloud-RAN," *IEEE Signal Processing Magazine*, vol. 31, no. 6, pp. 35–44, 2014. 1

[3] C.-Y. Chang, R. Schiavi, N. Nikaein, T. Spyropoulos, and C. Bonnet, "Impact of packetization and functional split on C-RAN fronthaul performance," in *2016 IEEE International Conference on Communications (ICC)*, 2016, pp. 1–7. 1

[4] V. Q. Rodriguez, F. Guillemin, A. Ferrieux, and L. Thomas, "Cloud-RAN functional split for an efficient fronthaul network," in *2020 International Wireless Communications and Mobile Computing (IWCMC)*, 2020, pp. 245–250. 1

[5] A. M. Alba, J. H. G. Velásquez, and W. Kellerer, "An adaptive functional split in 5G networks," in *IEEE INFOCOM 2019 - IEEE Conference on Computer Communications Workshops (INFOCOM WKSHPS)*, 2019, pp. 410–416. 1, 13, 17

[6] 3GPP, "TR 38.801, Study on new radio access technology: Radio access architecture and interfaces (Release 14)," 3rd Generation Partnership Project, Tech. Rep. V14.0.0, 03 2017, technical Specification Group Radio Access Network. [Online]. Available: https://www.3gpp.org/ftp/Specs/archive/38_series/38.801/38801-e00.zip 1, 13, 14, 16, 17

[7] M. Sousa, A. Alves, P. Vieira, M. P. Queluz, and A. Rodrigues, "Analysis and Optimization of 5G Coverage Predictions Using a Beamforming Antenna Model and Real Drive Test Measurements," *IEEE Access*, vol. 9, pp. 101 787–101 808, 2021. 2

[8] O. Dousse and P. Thiran, "Connectivity vs capacity in dense ad hoc networks," in *IEEE INFOCOM 2004*, vol. 1, March 2004, p. 486. 2

[9] J. Liu, W. Xiao, and A. C. K. Soong, *Dense networks of small cells*. Cambridge University Press, 2015, p. 96–121. 2

[10] ITU, "Guidelines for evaluation of radio interface technologies for IMT-2020," ITU, Tech. Rep. Report ITU-R M.2412-0, 11 2017. [Online]. Available: https://www.itu.int/dms_pub/itu-r/opb/rep/R-REP-M.2412-2017-PDF-E.pdf 2, 22, 23, 27, 31

[11] Ericsson, *Ericsson Mobility Report*, 2022. [Online]. Available: https://www.ericsson.com/49d3a0/assets/local/reports-papers/mobility-report/documents/2022/ericsson-mobility-report-june-2022.pdf 2, 3

[12] S. Ahmadi, "Introduction and background," in *5G NR*, S. Ahmadi, Ed. Academic Press, 2019, pp. xxv–xcvii. [Online]. Available: https://www.sciencedirect.com/science/article/pii/B978008102267200018X 2, 3

[13] P. Marsch, Ömer Bulakci, O. Queseth, and M. Boldi, *Introduction and Motivation*, 2018, pp. 1–13. 3

[14] 3GPP. (2018) About 3GPP. [Online]. Available: https://www.3gpp.org/about-3gpp 3

[15] 3GPP, "Release 15," 3rd Generation Partnership Project (3GPP), Tech. Rep., 04 2019. [Online]. Available: https://www.3gpp.org/release-15 3, 4

[16] V. Frascolla, *What Are 3GPP 5G Phase 1 and 2 and What Comes After*, 05 2020, pp. 385–398. 3

[17] A. EL RHAYOUR and T. MAZRI, "5G Architecture: Deployment scenarios and options," in *2019 International Symposium on Advanced Electrical and Communication Technologies (ISAECT)*, 2019, pp. 1–6. 3

[18] 3GPP, "Release 16," 3rd Generation Partnership Project (3GPP), Tech. Rep., 07 2020. [Online]. Available: https://www.3gpp.org/release-16 4

[19] J. Penttinen, *5G Second Phase Explained: The 3GPP Release 16 Enhancements*. John Wiley & Sons, Incorporated, 2021. [Online]. Available: https://books.google.pt/books?id=wEobzgEACAAJ 4

[20] N. Instruments. (2018) 3GPP Release 15 Overview. [Online]. Available: https://spectrum.ieee.org/scientists-build-ventricle-on-a-chip-to-study-heart-disease 4

[21] 3GPP, "Release 17," 3rd Generation Partnership Project (3GPP), Tech. Rep., 07 2020. [Online]. Available: https://www.3gpp.org/release-17 4

[22] ——, "Release 17 Description; Summary of Rel-17 Work Items (Release 17)," 3rd Generation Partnership Project, Tech. Rep. V1.0.0, Sep. 2022. [Online]. Available: https://www.3gpp.org/ftp/Specs/archive/21_series/21.917/21917-100.zip 4

[23] X. Lin, "An Overview of 5G Advanced Evolution in 3GPP Release 18," 2022. [Online]. Available: https://arxiv.org/abs/2201.01358 4

[24] 3GPP, "Release 18," 3rd Generation Partnership Project (3GPP), Tech. Rep. [Online]. Available: https://www.3gpp.org/release18 4

[25] H. Ramazanali, A. Mesodiakaki, A. Vinel, and C. Verikoukis, "Survey of user association in 5G HetNets," in *2016 8th IEEE Latin-American Conference on Communications (LATINCOM)*, 2016, pp. 1–6. 5

[26] C. Hoymann, W. Chen, J. Montojo, A. Golitschek, C. Koutsimanis, and X. Shen, "Relaying operation in 3GPP LTE: challenges and solutions," *IEEE Communications Magazine*, vol. 50, no. 2, pp. 156–162, 2012. 5

[27] H. R. Barzegar, N. El Ioini, V. T. Le, and C. Pahl, “Wireless Network Evolution Towards Service Continuity in 5G enabled Mobile Edge Computing,” 04 2020, pp. 78–85. 5

[28] T. Nguyen. (2017) Small Cell Networks and the Evolution of 5G (Part 1). [Online]. Available: https://www.qorvo.com/design-hub/blog/small-cell-networks-and-the-evolution-of-5g 5

[29] A. Damnjanovic, J. Montojo, Y. Wei, T. Ji, T. Luo, M. Vajapeyam, T. Yoo, O. Song, and D. Malladi, “A survey on 3GPP heterogeneous networks,” *IEEE Wireless Communications*, vol. 18, no. 3, pp. 10–21, 2011. 5

[30] K. Sharma, “Comparison of energy efficiency between macro and micro cells using energy saving schemes,” Master’s thesis, Lund University, 2017. 5

[31] A. R. Ramos, “Cellular Planning and Optimization for 4G and 5G Mobile Networks,” Master’s thesis, Universidade da Beira Interior, 2019. 5, 21, 31

[32] 3GPP, “TS 22.105, Services and service capabilities (Release 17),” 3rd Generation Partnership Project, Tech. Rep. V17.0.0, March 2022. [Online]. Available: https://www.3gpp.org/ftp/Specs/archive/22_series/22.105/22105-h00.zip 6, 33

[33] Y. S. Othman, M. H. Megahed, M. A. Rezka, and F. A. E. Amer, “A New Communication Protocol for Drones Cooperative Network: 5G Site Survey Case Study,” *International Journal of Advanced Computer Science and Applications*, vol. 12, no. 6, 2021. [Online]. Available: http://dx.doi.org/10.14569/IJACSA.2021.0120616 9

[34] M. A. Habibi, M. Nasimi, B. Han, and H. D. Schotten, “A Comprehensive Survey of RAN Architectures Toward 5G Mobile Communication System,” *IEEE Access*, vol. 7, pp. 70 371–70 421, 2019. 9

[35] P. M. C. Marques, “Ethernet-based C-RAN fronthaul,” Master’s thesis, Universidade de Aveiro, 2018. 9

[36] E. Jordan. (2021) Open RAN functional splits, explained. [Online]. Available: https://www.5gtechnologyworld.com/open-ran-functional-splits-explained/ 9, 15

[37] D. T. Kiet, T. M. Hieu, N. Q. Hung, N. Van Cuong, V. T. Van, and P. N. Cuong, “Research and Implementation of eCPRI Processing Module for Fronthaul Network on FPGA in 5G – NR gNodeB Base Station,” in *2020 4th International Conference on Recent Advances in Signal Processing, Telecommunications Computing (SigTelCom)*, 2020, pp. 1–5. 9, 11

[38] H. Niu, C. Li, A. Papathanassiou, and G. Wu, “RAN architecture options and performance for 5G network evolution,” in *2014 IEEE Wireless Communications and Networking Conference Workshops (WCNCW)*, 2014, pp. 294–298. 9, 11

[39] O. Andersson. (2021) Functional Splits: the foundation of an Open 5G RAN. [Online]. Available: https://www.5gtechnologyworld.com/functional-splits-the-foundation-of-an-open-5g-ran/ 11, 14, 15

[40] "CPRI Specification V7.0," CPRI and Ericsson AB and Huawei Technologies Co. Ltd and NEC Corporation and Alcatel Lucent and Nokia Networks, Tech. Rep., 2015. [Online]. Available: http://www.cpri.info/downloads/CPRI_v_7_0_2015-10-09.pdf 11, 12

[41] K. Murphy, "Centralized RAN and Fronthaul," Ericsson, Tech. Rep., 2015. 11

[42] ITU-T, "SERIES G: TRANSMISSION SYSTEMS AND MEDIA, DIGITAL SYSTEMS AND NETWORKS," ITU, Tech. Rep. ITU-T Recommendation G.Sup66, 09 2020. [Online]. Available: https://www.itu.int/rec/T-REC-G.Sup66-202009-I/en 11

[43] "eCPRI Specification V2.0," CPRI and Ericsson AB and Huawei Technologies Co. Ltd and NEC Corporation and Nokia, Tech. Rep., 2019. [Online]. Available: http://www.cpri.info/downloads/eCPRI_v_2.0_2019_05_10c.pdf 11, 12, 13, 17

[44] L. M. P. Larsen, A. Checko, and H. L. Christiansen, "A Survey of the Functional Splits Proposed for 5G Mobile Crosshaul Networks," *IEEE Communications Surveys Tutorials*, vol. 21, no. 1, pp. 146–172, 2019. 13, 14, 15, 16

[45] G. Kalfas, M. Agus, A. Pagano, L. A. Neto, A. Mesodiakaki, C. Vagionas, J. Vardakas, E. Datsika, C. Verikoukis, and N. Pleros, "Converged Analog Fiber-Wireless Point-to-Multipoint Architecture for eCPRI 5G Fronthaul Networks," in *2019 IEEE Global Communications Conference (GLOBECOM)*, 2019, pp. 1–6. 13

[46] A. Sharma. (2021) Exploring functional splits in 5G RAN: Tradeoffs and use cases. [Online]. Available: https://www.rcrwireless.com/20210317/opinion/readerforum/exploring-functional-splits-in-5g-ran-tradeoffs-and-use-cases-reader-forum 14, 15, 16

[47] CMCC, "Transport requirement for CU and DU functional splits options," 3rd Generation Partnership Project, Tech. Rep., 08 2016, discussion. [Online]. Available: https://www.3gpp.org/ftp/tsg_ran/WG3_Iu/TSGR3_93/Docs/R3-161813.zip 15

[48] D. Harutyunyan, R. Riggio, S. Kuklinski, and T. Ahmed, "CU placement over a reconfigurable wireless fronthaul in 5G networks with functional splits," *Int. Journal of Network Management*, vol. 30, no. 1, 2020. [Online]. Available: https://doi.org/10.1002/nem.2086 15

[49] S. C. Forum, "Document 159.07.02, Small cell virtualization functional splits and use cases (Release 7.0)," Small Cell Forum, Tech. Rep. V14.0.0, 01 2016. [Online]. Available: https://scf.io/en/download.php?doc=159 16, 17

[50] A. Tukmanov, "Fronthauling for 5G and beyond," pp. 139–168, 2017. [Online]. Available: https://digital-library.theiet.org/content/books/10.1049/pbte074e_ch7 16, 17

[51] Q. Han, C. Wang, M. Levorato, and O. Simeone, "On the Effect of Fronthaul Latency on ARQ in C-RAN Systems," 10 2015. 16

[52] I. NTT DOCOMO, “R3-162102, CU-DU split: Refinement for Annex A (Transport network and RAN internal functional split),” 3rd Generation Partnership Project, Tech. Rep., 10 2016, discussion. [Online]. Available: https://www.3gpp.org/ftp/tsg_ran/WG3_Iu/TSGR3_93bis/Docs/R3-162102.zip 16

[53] I. A. Alimi, A. L. Teixeira, and P. P. Monteiro, “Toward an Efficient C-RAN Optical Fronthaul for the Future Networks: A Tutorial on Technologies, Requirements, Challenges, and Solutions,” *IEEE Communications Surveys Tutorials*, vol. 20, no. 1, pp. 708–769, 2018. 17

[54] C. Harper and S. Sirotkin, *NG-RAN Architecture*, 2020, pp. 123–234. 17

[55] M. Klinkowski, D. Wypiór, and I. Michalski, “Open RAN—Radio Access Network Evolution, Benefits and Market Trends,” *Applied Sciences*, 2022. 17, 18, 20

[56] A. U. T. Yajima, T. Uchino, and S. Okuyama, “Overview of O-RAN Fronthaul Specifications,” 2019. 17, 18

[57] S. Lagén, L. Giupponi, A. Hansson, and X. Gelabert, “Modulation Compression in Next Generation RAN: Air Interface and Fronthaul Trade-offs,” *IEEE Communications Magazine*, vol. 59, no. 1, pp. 89–95, 2021. 18

[58] “O-RAN: Towards an Open and Smart RAN,” O-RAN Alliance, Tech. Rep., 2018. [Online]. Available: https://static1.squarespace.com/static/5ad774cce74940d7115044b0/t/5bc79b371905f4197055e8c6/1539808057078/O-RAN+WP+FInal+181017.pdf 18, 19

[59] M. F. Erik Westerberg. (2020) The innovation potential of Non Real-time RAN Intelligent Controller. [Online]. Available: https://www.ericsson.com/en/blog/2020/10/innovation-potential-of-non-real-time-ran-intelligent-controller 18

[60] “O-RAN Working Group 2 (Non-RT RIC and A1 interface WG); A1 interface: General Aspects and Principles,” O-RAN ALLIANCE, Tech. Rep. O-RAN.WG2.A1GAP-v02.03, 10 2021. [Online]. Available: https://orandownloadsweb.azurewebsites.net/specifications 18

[61] “O-RAN Architecture Description,” O-RAN ALLIANCE, Tech. Rep. O-RAN.WG1.O-RAN-Architecture-Description-v06.00, 3 2022. [Online]. Available: https://orandownloadsweb.azurewebsites.net/specifications 18

[62] “O-RAN Near-Real-time RAN Intelligent Controller Architecture & E2 General Aspects and Principles 2.01,” O-RAN ALLIANCE, Tech. Rep. O-RAN.WG3.E2GAP-v02.01, 3 2022. [Online]. Available: https://orandownloadsweb.azurewebsites.net/specifications 18

[63] M. Ma. (2019) Open RAN: Catalyzing 5G Use Case Innovations. [Online]. Available: https://www.thefastmode.com/expert-%20opinion/15608-open-ran-catalyzing-5g-use-case-innovations 20

[64] "O-RAN Use Cases and Deployment Scenarios," O-RAN Alliance, Tech. Rep., 2020. [Online]. Available: https://www.o-ran.org/s/O-RAN-Use-Cases-and-Deployment-Scenarios-Whitepaper-February-2020.pdf 20

[65] 3GPP, "User Equipment (UE) radio transmission and reception; Part 1: Range 1 Standalone (Release 17)," 3rd Generation Partnership Project, Tech. Rep. V17.6.0, June 2022. [Online]. Available: https://www.3gpp.org/ftp/Specs/archive/38_series/38.101-1/38101-1-h60.zip 20

[66] H. Hämäläinen, "Uplink data measurement and analysis for 5G eCPRI radio unit," Master's thesis, University of Oulu, 2020. 20, 21

[67] I. M. P. Gonçalves, "Small-Cell LTE Networks: Evaluating RF Planning Methods," Master's thesis, Instituto Superior Técnico, 2018. 21

[68] X. Chu, D. Lopez-Perez, Y. Yang, and F. Gunnarsson, *Heterogeneous cellular networks: theory, simulation and deployment*. Cambridge University Press, 2013. 21, 22

[69] S. Sousa, F. J. Velez, and J. M. Peha, "Impact of propagation model on capacity in small-cell networks," in *2017 International Symposium on Performance Evaluation of Computer and Telecommunication Systems (SPECTS)*, 2017, pp. 1–8. 21

[70] F. Letourneux, S. Guivarch, and Y. Lostanlen, "Propagation models for Heterogeneous Networks," in *2013 7th European Conference on Antennas and Propagation (EuCAP)*, 2013, pp. 3993–3997. 21

[71] R. R. Paulo and F. J. Velez, "System Level Simulation of Urban Micro-cellular 4G Scenarios in the Sub-6 GHz Frequency Bands," in *2021 Telecoms Conference (ConfTELE)*, 2021, pp. 1–6. 22

[72] ITU-R, "IMT Vision – Framework and overall objectives of the future development of IMT for 2020 and beyond," ITU, Tech. Rep. Report ITU-R M.2083-0, 09 2015. [Online]. Available: https://www.itu.int/dms_pubrec/itu-r/rec/m/R-REC-M.2083-0-201509-I!!PDF-E.pdf 22

[73] F. Baccelli and X. Zhang, "A correlated shadowing model for urban wireless networks," in *2015 IEEE Conference on Computer Communications (INFOCOM)*, 2015, pp. 801–809. 23

[74] K. McTiernan. (2020) Sidelink and Its Impact on Lawful Intelligence. [Online]. Available: https://www.ss8.com/sidelink-and-its-impact-on-lawful-intelligence 24

[75] *3GPP TS 138.214 version 15.3.0 Release 15, 5G, NR, Physical Layer Procedures for Data*, 3rd Generation Partnership Project, Oct. 2018, technical Specification Group Radio Access Network. 25

[76] S. Martiradonna, A. Grassi, G. Piro, and G. Boggia, "5G-air-simulator: An open-source tool modeling the 5G air interface," *Computer Networks*, vol. 173, p. 107151, 2020. [Online]. Available: https://www.sciencedirect.com/science/article/pii/S1389128619317359 27

[77] 5G-air-simulator official repository, "5G-air-simulator," 2020. [Online]. Available: https://github.com/telematics-lab/5G-air-simulator 27

[78] G. Piro, L. A. Grieco, G. Boggia, F. Capozzi, and P. Camarda, "Simulating LTE Cellular Systems: An Open-Source Framework," *IEEE Transactions on Vehicular Technology*, vol. 60, no. 2, pp. 498–513, 2011. 27, 40

[79] S. Martiradonna, A. Grassi, G. Piro, and G. Boggia, "Understanding the 5G-air-simulator: A tutorial on design criteria, technical components, and reference use cases," *Computer Networks*, vol. 177, p. 107314, 2020. [Online]. Available: https://www.sciencedirect.com/science/article/pii/S1389128619317347 27, 28, 33, 38

[80] R. R. Paulo and F. J. Velez, "5G-air-simulator_ITU-R_M-2412-0," https://github.com/RRP-IT/5G-air-simulator_ITU-R_M-2412-0.git, 2022. 27

[81] G. Miao, J. Zander, K. Sung, and S. Slimane, *Fundamentals of mobile data networks*, 01 2016. 28, 29

[82] I.-S. Comsa, A. De-Domenico, and D. Ktenas, "QoS-Driven Scheduling in 5G Radio Access Networks - A Reinforcement Learning Approach," in *GLOBECOM 2017 - 2017 IEEE Global Communications Conference*, 2017, pp. 1–7. 29

[83] A. Mamane, M. Fattah, M. E. Ghazi, M. E. Bekkali, Y. Balboul, and S. Mazer, "Scheduling Algorithms for 5G Networks and Beyond: Classification and Survey," *IEEE Access*, vol. 10, pp. 51 643–51 661, 2022. 29

[84] Y. Li, E. Pateromichelakis, N. Vucic, J. Luo, W. Xu, and G. Caire, "Radio Resource Management Considerations for 5G Millimeter Wave Backhaul and Access Networks," *IEEE Communications Magazine*, vol. 55, no. 6, pp. 86–92, 2017. 29

[85] M. Fuentes, J. Carcel, C. Dietrich, L. Yu, E. Garro, P. Volker, F. Lazarakis, O. Grondalen, O. Bulakci, J. Yu, W. Mohr, and D. Gomez-Barquero, "5G New Radio Evaluation Against IMT-2020 Key Performance Indicators," *IEEE Access*, vol. 8, p. 110896, 06 2020. 29

[86] M. Nasralla and M. Martini, "Content-aware downlink scheduling for LTE wireless systems: A survey and performance comparison of key approaches," *Computer Communications*, vol. 130, 09 2018. 29

[87] R. Paulo and F. Velez, "An Extensive Study on the Performance Evaluation and Scheduling of HeNBs," *IEEE Access*, vol. PP, pp. 1–1, 03 2021. 30

[88] S. Sousa, F. J. Velez, and J. M. Peha, "Impact of considering the ITU-R two slope propagation model in the system capacity trade-off for LTE-A HetNets with small cells," in

2017 XXXIInd General Assembly and Scientific Symposium of the International Union of Radio Science (URSI GASS), Aug 2017, pp. 1–4. 30

[89] 3GPP, "TS 38.101-1, User Equipment (UE) radio transmission and reception; Part 1: Range 1 Standalone (Release 17)," 3rd Generation Partnership Project, Tech. Rep. V17.5.0, March 2022. [Online]. Available: https://www.3gpp.org/ftp/Specs/archive/38_series/38.101-1/38101-1-h50.zip 30

[90] 3GPP, "TS 38.211 V17.1.0, NR; Physical channels and modulation (Release 17)," 3rd Generation Partnership Project, Tech. Rep. V17.1.0, March 2022. [Online]. Available: https://www.3gpp.org/ftp/Specs/archive/38_series/38.211/38211-h10.zip 31

[91] M. M. Nasralla, "A Hybrid Downlink Scheduling Approach for Multi-Traffic Classes in LTE Wireless Systems," *IEEE Access*, vol. 8, pp. 82 173–82 186, 2020. 31

[92] A. B. Sediq, R. H. Gohary, and H. Yanikomeroglu, "Optimal tradeoff between efficiency and Jain's fairness index in resource allocation," in *2012 IEEE 23rd International Symposium on Personal, Indoor and Mobile Radio Communications - (PIMRC)*, Sep. 2012, pp. 577–583. 33

[93] Y. L. Lee, J. Loo, and T. C. Chuah, "Chapter 24 - Modeling and performance evaluation of resource allocation for LTE femtocell networks," in *Modeling and Simulation of Computer Networks and Systems*, M. S. Obaidat, P. Nicopolitidis, and F. Zarai, Eds. Boston: Morgan Kaufmann, 2015, pp. 683–716. [Online]. Available: https://www.sciencedirect.com/science/article/pii/B9780128008874000249 33

[94] B. Gavish and S. Sridhar, "Economic aspects of configuring cellular networks," *Wireless Networks*, vol. 1, pp. 115–128, 1995. 44, 45

[95] F. J. Velez and L. M. Correia, "Optimisation of Mobile Broadband Multi-Service Systems Based in Economics Aspects," *Wireless Networks*, vol. 9, no. 5, pp. 525–533, Sep 2003. [Online]. Available: https://doi.org/10.1023/A:1024696318236 45

[96] F. J. Velez, O. Cabral, F. Merca, and V. Vassiliou, "Service characterization for cost/benefit optimization of enhanced UMTS," *Telecommunication Systems*, vol. 50, no. 1, pp. 31–45, Apr 2012. [Online]. Available: https://doi.org/10.1007/s11235-010-9383-2 45

[97] K. Johansson, A. Furuskar, P. Karlsson, and J. Zander, "Relation between base station characteristics and cost structure in cellular systems," in *2004 IEEE 15th International Symposium on Personal, Indoor and Mobile Radio Communications (IEEE Cat. No.04TH8754)*, vol. 4, Sep. 2004, pp. 2627–2631 Vol.4. 45

[98] Moniem-Tech. (2022) Why 7.2x split is the Best Split Option? [Online]. Available: https://moniem-tech.com/2022/03/13/why-7-2x-split-is-the-best-split-option/ 46

[99] HUBER+SUHNER. (2019) 5G Fundamentals: Functional Split Overview. [Online]. Available: https://www.hubersuhner.com/en/documents-repository/technologies/pdf/fiber-optics-documents/5g-fundamentals-functional-split-overview 46